Higher Normal School of Technological Education of Skikda
Department of physics and chemistry

Dissertation

submitted for the degree of education:

Degree of Middle School Teacher

Double half-Heusler Compounds: Novel High Efficiency Thermoelectric Materials for Energy Applications

---

By:

Assil Dergal
Nour Djihane Slougui

Name	Role	Institution
Pr. Abdelmalek Khorief Nacereddine	President	Higher School of Technological Education - Skikda
Dr. Mohamed Diaf	Supervisor	Higher School of Technological Education - Skikda
Dr. Fayçal Oumelaz	Examinator	Higher School of Technological Education - Skikda

---

academic year **2024/2025**

Contents

List of Figures

List of Tables

List of Equations

Abstract/Résumé

This dissertation presents a theoretical investigation of three titanium-based double half-Heusler compounds: $Ti_2OsNiSb_2$, $Ti_2OsPtSb_2$, and $Ti_2OsPdSb_2$, using first-principles DFT calculations via Quantum ESPRESSO packadge. The optimized lattice parameters confirm a stable tetragonal structure with c/a ratio ≈ 2.00, indicating minimal distortion compared to the cubic half-Heusler phase. The calculated lattice constants are respectively: 6.086Å for $Ti_2OsNiSb_2$; 6.207Å for $Ti_2OsPtSb_2$; and 6.194Å for $Ti_2OsPdSb_2$. with negative formation energies confirming structural stability.

Cette dissertation présente une étude théorique de trois composés double half-Heusler à base de titane: $Ti_2OsNiSb_2$, $Ti_2OsPtSb_2$, et $Ti_2OsPdSb_2$ — en utilisant des calculs ab initio basés sur la théorie de la fonctionnelle de la densité (DFT) via le code Quantum ESPRESSO. Les paramètres de maille optimisés confirment une structure tétragonale stable avec un rapport $c/a \approx 2.00$, indiquant une faible distorsion par rapport à la phase half-Heusler cubique. Les constantes de maille calculées sont respectivement : 6.086Å pour $Ti_2OsNiSb_2$, 6.207Å pour $Ti_2OsPtSb_2$ et 6.194Å pour $Ti_2OsPdSb_2$. Les énergies de formation négatives confirment la stabilité structurale de ces composés.

Acknowledgment

*We praise **Allah Almighty** who enabled us to accomplish this humble work.*

Our thanks and deepest gratitude to our Supervisor, **Dr Mohamed Diaf**, who made this work possible, his invaluable guidance, advices, patience and encouragement were instrumental in shaping this dissertation.

We sincerely thank the members of our jury, the jury president, **Pr. Abdelmalek Khorief Nacereddine**, and the Examiner, **Dr. Fayçal Oumelaz** who honored us by accepting to evaluate our dissertation. We are grateful for their time, their insightful comments, and their constructive suggestions, which contributed to the enrichment of this modest work.

We are also thankful to all the professors and staff of the Higher School of Teachers in Skikda, especially those from the Physics Department, for their dedication and the knowledge they shared during our academic journey.

We would like to express our warmest thanks to our beloved **parents**, for their unconditional love, trust, and constant support.

From childhood friends and cousins to academic partners, from shared dreams to late-night research sessions, we walked this road as one, bound by love, faith, and purpose. We thank each other for every word of encouragement, every quiet strength, every laugh that softened the rough path.

More than a dissertation, it is a testament to our journey, effort, resilience and sisterhood, heart to heart, hand in hand.

Assil & Djihane

1

Heusler compounds

With the increasing global need for efficient energy conversion and sustainable power sources, thermoelectric materials have gained significant attention for their ability to directly transform heat into electricity. Among these materials, double Half-Heusler (DHH) compounds represent a novel and promising class due to their tunable electronic properties, thermal stability, and structural versatility. This research aims to critically analyze the electronic structure, thermal transport mechanisms, and charge-carrier dynamics of DHH compounds to assess their suitability for high-efficiency thermoelectric applications especially their ability to enhance energy conversion efficiency. Traditional thermoelectric materials often suffer from a trade-off between electrical conductivity and thermal conductivity, that hampers their efficiency. However, DHH compounds offer an interesting alternative, as they combine the advantageous characteristics of both Half-Heusler and full-Heusler structures, potentially achieving an optimized balance between electrical conductivity, Seebeck coefficient, and thermal conductivity. Thus through computational modeling, experimental synthesis, and advanced characterization techniques, we seek to identify methods of optimizing their power factor and reducing lattice thermal conductivity. resulting in expanding the understanding of DHH-based thermoelectrics, this study contributes to the development of next-generation energy-harvesting materials, that can potentially be used for waste heat harvesting, portable power, and green energy systems.

1.1 Heusler compounds

1.1.1 Historical overview

The discovery of Heusler compounds in 1903 by Friedrich Heusler revolutionized the field of magnetism by revealing that ferromagnetic alloys could be formed from non-magnetic elements, such as(Cu_2MnAl) [1](Fig.1.1). By the mid-20th century, advancements in X-ray diffraction had established the cubic$L2_1$ structure (general formula X_2YZ) [2–4]. The magnetic behavior was attributed to RKKY exchange interactions [5,6], where indirect exchange between manganese atoms is mediated by conduction electrons. During the 1970s and 1980s, research expanded beyond magnetism, identifying semiconducting Heusler alloys (e.g., NiTiSn, CoTiSb) [7,8] and half-Heusler compounds ($C1_b$ structure) with one fewer X atom [9,10] such as TiNiSn, ZrNiSn and HfNiSn which exhibited tunable electronic

properties and thermoelectric potential [11], broadening their applications in electronics and energy materials [12–14].

In the 21st century, interest in Heusler and half-Heusler compounds surged due to their potential in cutting-edge technologies. They have been extensively studied for thermoelectric applications, with efforts focused on reducing lattice thermal conductivity through doping [15, 16], alloying [17] and nanostructuring [18, 19]. Additionally, certain Heusler compounds have been found to exhibit topological insulating behavior, characterized by conductive surface states coexisting with an insulating bulk. This unique property positions them as promising candidates for quantum computing and next-generation electronics [20]. Advances in computational methods, particularly high-throughput screening based on Density Functional Theory (DFT) [21–23], along with progress in fabrication techniques like spark plasma sintering (SPS) and molecular beam epitaxy, have further propelled the field [24, 25]. Co-based Heusler alloys have shown significant potential in spintronics, owing to their high Curie temperatures and spin polarization. In parallel, half-Heusler compounds remain a focus in thermoelectric research for achieving high ZT values in energy harvesting. By 2016, the "Heusler 4.0" era highlighted over 1,000 multifunctional variants, each exhibiting exceptional electronic, magnetic and thermoelectric properties. This era underscores the adaptability, chemical stability, and diverse functionalities of Heusler compounds, reinforcing their importance in next-generation energy systems, electronic devices, and quantum technologies [26].

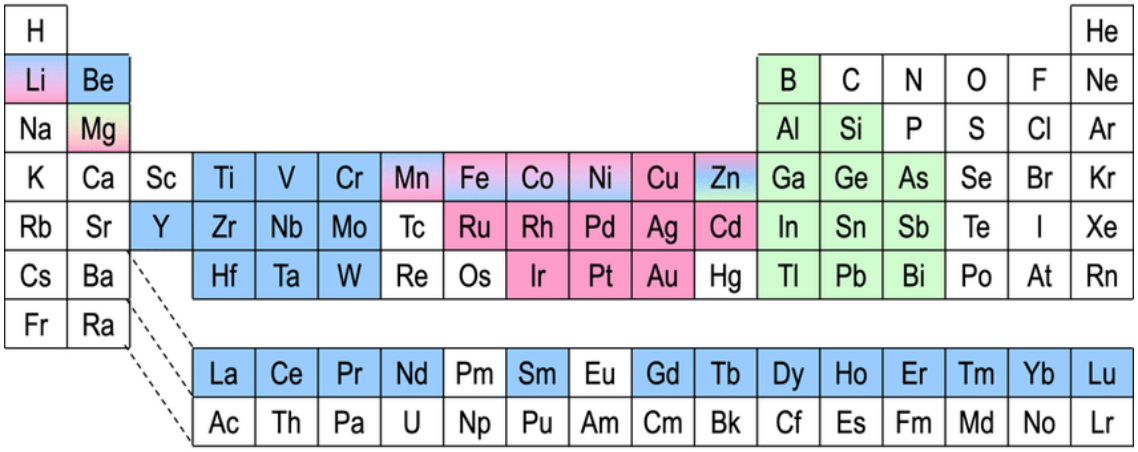

Figure 1.1: periodic table highlighting the possible combinations of elements in Heusler compounds [27]

.

1.1.2 Types of Heusler coumpounds

Heusler coumpounds are classified into three main types (Full Heusler, half Heusler , and inverse heusler) based on their crystallographic structures and chemical compositions. The Full Heusler compounds (FHC) are intermetallic materials with the general chemical formula X_2YZ, where X and Y are transition metals or lanthanides, and Z is a main-group element or semimetal. They crystallize

in a face-centered cubic (FCC) structure with space group $Fm\bar{3}m$ (No. 225) , forming a highly ordered $L2_1$ arrangement. The crystal structure consists of four interpenetrating FCC sublattices , with X atoms occupying Wyckoff position 8c, Y atoms at 4a, and Z atoms at 4b [11,28](Fig. 1.2). The electronic structure of FHC arises from strong d-orbital hybridization between the X and Y atoms, with contributions from the p-orbitals of the Z element [29] [30], leading to unique band structures that enable half-metallicity, making theses compounds ideal for spintronics [31]. Regarding their thermoelectric properties, these stem from their ability to balance electrical and thermal conductivity, facilitating efficient heat-to-electricity conversion [32] [33]. Many FHC compounds exhibit high Curie temperatures (>300 K) [34], which ensures stable magnetic properties at room temperature [35]. Some also demonstrate shape memory effects, allowing them to revert to their original shape response to thermal or magnetic stimuli [36] [35].

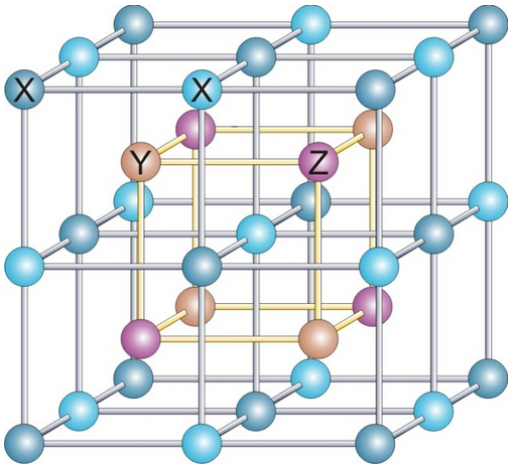

Figure 1.2: Face-centered cubic lattice of full Heusler compounds [37].

Half-Heusler compounds are a ternary intermetallic materials with the general formula XYZ, where X and Y are transition metals, and Z is a main group element. They crystallize in a cubic $MgAgAs$-type structure (space group $F\bar{4}3m$, No. 216) [38] exhibiting a highly ordered $C1_b$ arrangement [11]. They feature three interpenetrating FCC sublattices (X: 4a, Y: 4b, Z: 4c) and a vacant 4d site [39](fig.1.3), enabling unique bonding and structural flexibility. The electronic properties of HH compounds arise from strong d-orbital hybridization between X and Y atoms [40], along with contributions from the p-orbitals of the Z element [41,42]. These interaction results in diverse electronic structures, often leading to semiconducting behavior with a tunable bandgap [43,44]. HH compounds excel in thermoelectrics [45] due to their high Seebeck coefficient, favorable electrical conductivity, and low thermal conductivity [11], Some HH compounds exhibit shape memory effects [11,46,47], as well as room-temperature magnetism ensuring stable functionality [48].

Inverse Heusler Compounds (IHC) are also intermetallic materials with the formula X_2YZ, where X and Y are transition metals, and Z is a main-group element [50]. Althought they share the

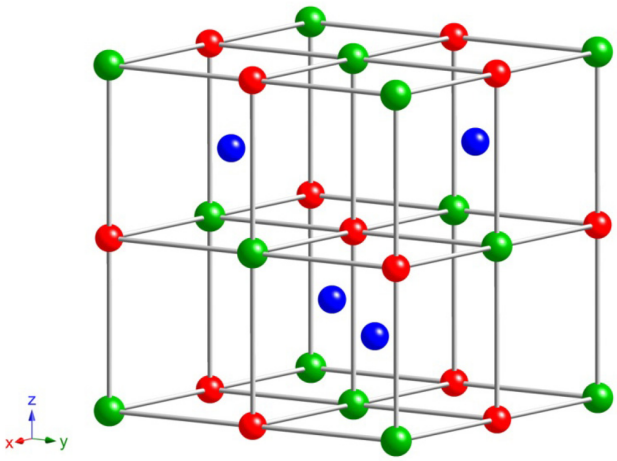

Figure 1.3: Face-centered cubic lattice of half-Heusler coumpounds [49]

.

same chemical formula as FHC, they exhibit an inverted atomic arrangement [51], leading to a face-centered cubic structure with space group $F\bar{4}3m$, No. 216) and a Hg_2CuTi-type ordering [11]. In this configuration, the transition metals occupy tetrahedral sites, while the main-group elements resides in octahedral sites [51]. The structure consists of four interpenetrating FCC sublattices with distinct atomic positions: X at 4a, X' (or a different transition metal) at 4c, Y at 4b , and Z at 4d [11, 52].The electronic properties of IHC are determined by strong d-d hybridization between X and Y atoms, along with p-d interactions with Z element [53], often resulting in half-metallic or semiconducting behavior [54]. Due to sublattice competition, many IHC exhibit altered spin polarization, making them promising candidates for spintronic applications [55]. Their reduced lattice symmetry enhances phonon scattering, which lowers thermal conductivity while maintaining electrical conductivity—key for thermoelectric applications [56], some compositions (e.g., Ni-Mn-based alloys), also exhibit room-temperature magnetic stability [57, 58], tunable band gaps and defect tolerance making them promising for energy conversion technologies, including thermoelectrics and solar cells [59].

1.2 Thermoelectricity

Thermoelectricity refers to the direct and thermodynamically reversible conversion between heat and electricity, combining two key phenomena in materials: heat transfer “thermo” and charge transfer “electricity”. It is encompassed by two differentiated effects named after their discoverers: the Seebeck and Peltier effects. The Seebeck effect, the first observed thermoelectric phenomenon, was initially discovered by Alessandro Volta in 1787 and later independently rediscovered and named by Thomas Johann Seebeck in 1821. The Peltier effect, discovered by French watchmaker and physicist Jean Charles Athanase Peltier, occurs when an electric current flows through the interface of two different materials, causing heat to be either absorbed or released. Both effects describe the movement of

electric charge in response to a temperature gradient.

1. **Seebeck effect:**

   Seebeck observed that connecting two different metals in a closed loop causes a needle to deflect when a temperature difference is applied between the junctions. Although Seebeck did not recognize that this phenomenon was due to the generation of an electric current (fig. 1.4), Ørsted later identified it and introduced the term 'thermoelectricity'. Since these initial discoveries, the Seebeck effect has been quantified as an electromotive force (e_s), which is directly proportional to the temperature gradient [60,61]. This relationship is mathematically expressed as:

   $$e_s = -\alpha_s \Delta T \tag{1.2}$$

   where α_s is seebek coefficient

2. **Peltier effect:** The Peltier effect, a complementary phenomenon to the Seebeck effect, describes the absorption or release of heat flux q_p at the junction of two dissimilar materials as an electric current flows across it (fig.1.4) [60]. This effect is expressed as:

   $$q_p = \Delta_{\alpha_p} j_e = T \Delta_{\alpha_s} j_e \tag{1.4}$$

   where Δ_{α_p} and Δ_{α_s} are the differences in the Peltier and Seebeck coefficients between the two materials, and j_e is the electric current density [62].

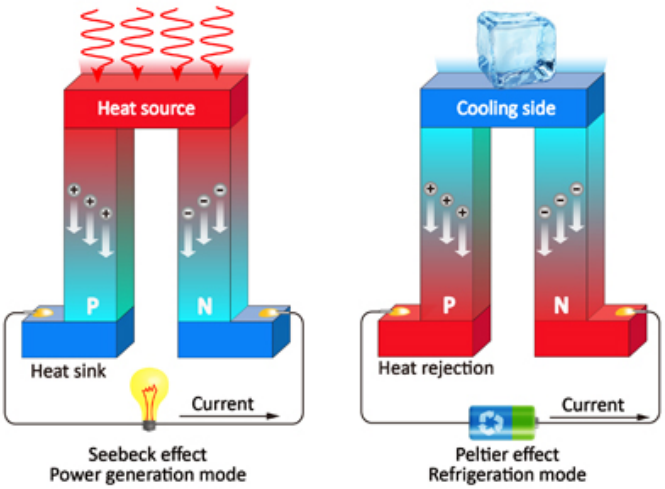

Figure 1.4: Seebeck and Peltier Effects in Thermoelectric Devices.

These thermoelectric phenomena are comprehensively explained through the Boltzmann transport equation (BTE), which allows the derivation of transport coefficients governing thermoelectric behavior.

Thermoelectric materials are widely classified into intermetallics, HH, oxides, Zintl-phase materials, pnictogens, nitrides, and their superlattice structures. These materials are typically degenerate semiconductors with complex band structures [63]. Recently, nanocomposites incorporating carbon nanomaterials and electronically conducting polymers have emerged as candidates for flexible, next-generation thermoelectric devices. However, their thermoelectric performances are much lower than those of classical inorganic materials [64].

1.2.1 Enhancing Thermoelectric Efficiency

Thermoelectric power generation (TEG) has been extensively studied as a clean energy conversion technology capable of harvesting waste heat and converting solar energy into electricity [65]. Carnot efficiency and dimensionless figure of merit characterize its efficiency and influence the feasibility, cost and power density of TE devices [60].

Nanotechnology has been explored by researchers to enhance TE efficiency since 1993 and this resulted in breakthroughs such as Venkatasubramanian's 2.4 ZT (2001), Harman's 3.2 Z_T (2002), and Kanatzidis' bulk ZT of 1.4 (2003). Enhancing the thermoelectric figure of merit involves fine-tuning the subtle interplay between lattice vibrations, charge transport, orbital configurations, and spin dynamics to enhance both electric performance and block thermal conductivity simultaneously. This multidisciplinary approach makes possible the development of high-performance materials with greatly improved energy conversion efficiency (fig.1.5).

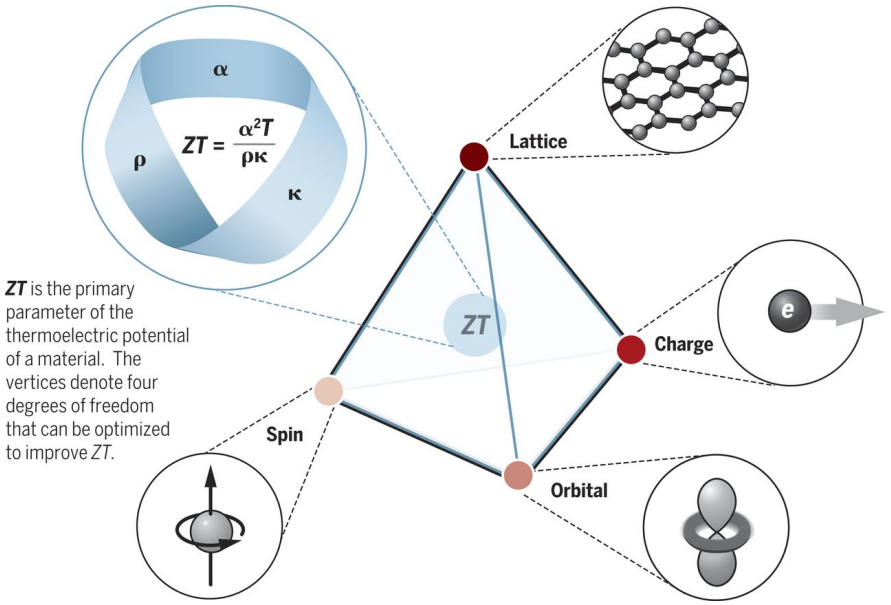

Figure 1.5: Enhancing ZT through the interplay of lattice, charge, orbital, and spin degrees of freedom [66].

The highest thermoelectric material efficiency is established by its figure of merit:

$$Z_T = \frac{S^2}{\rho k} T \tag{1.6}$$

Where S is the Seebeck coefficient, ρ is the electrical resistivity, k is the thermal conductivity and T is the absolute temperature of the material at the point in question [67].

These combined doping strategies—tuning carrier concentration and enhancing phonon scattering—have significantly improved ZT, achieving values of up to ∼1 for n-type HH materials and ∼0.5 for p-type counterparts. Additionally, these materials show excellent thermal stability at temperatures up to 900 K (fig.1.6) [49].

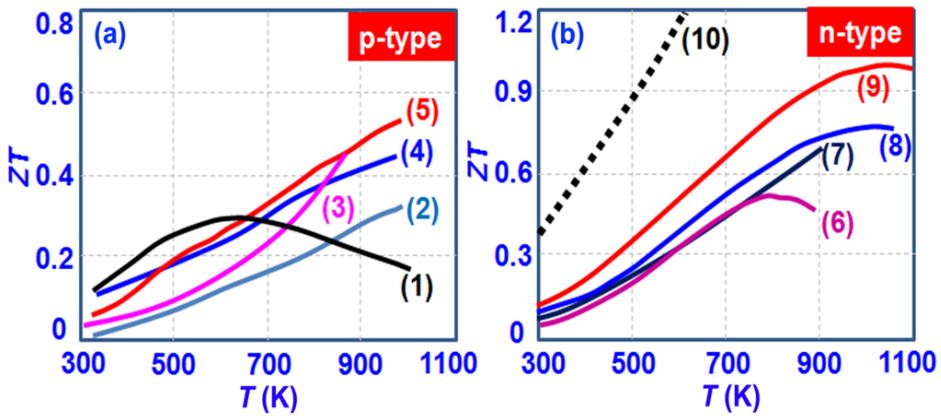

Figure 1.6: Performance Comparison of n- and p-Type HH Compounds [49].

To further enhance thermoelectric (TE) performance, researchers are exploring four key strategies: improving material ZT, optimizing design to minimize parasitic losses, investigating alternative thermodynamic cycles, and advancing heat exchange systems. These efforts could potentially double TE efficiency, although practical application remains under development [63, 66, 68].

1.3 Thermoelectricity and Heusler Compounds:

Thermoelectric materials thus offer a promising route for energy conversion between waste heat and electricity and, conversely, based on the Seebeck and Peltier effects. The efficiency of a thermoelectric material is determined by the dimensionless figure of merit. Achieving a high Z_T requires a material that combines a high Seebeck coefficient and electrical conductivity with low thermal conductivity—a challenge in itself since these are interdependent parameters. In this context, Heusler compounds have gained significant interest as potential thermoelectric materials due to their tunable electronic structures, mechanical robustness, and thermal stability. These intermetallic compounds, even though composed of metallic elements, can be semiconducting in nature and structurally flexible, thus are susceptible to systematic optimization of transport properties [69].

Heusler compounds, including full-Heusler, half-Heusler, inverse, and more recently double half-Heusler compounds, exhibit enormous variability of electronic and thermal behavior depending on their atomic structure and composition. Band structure tailoring through doping and elemental substitution enables control of power factor($S^2\sigma$). Furthermore, strategies like alloying and nanostructuring have proven effective in reducing lattice thermal conductivity by enhancing phonon scattering.

For instance, the n-type half-Heusler compound TiNiSn showed a ZT of around 0.5 at 700 K, even without carrier tuning through alloying [70]. Power factor and ZT are further enhanced by techniques like carbon/nitrogen addition, achieving $ZT \approx 0.7$ at 723 K [71]. Even greater, substitutions such as Cu interstitial doping have increased ZT to 0.9 at 773 K [72].

On the p-type side, FeNbSb-based alloys have attained $Z_T > 1.0$ near 1100 K through band Ti substitution and engineering [73]. Other compounds have achieved $ZT \approx 1.5$ at 1200 K, through band Ti substitution and engineering [74].

Broader half-Heusler systems such as (Ti,Zr,Hf)NiSn solid solutions always achieve Z_T values around 1.0, the best compositions (e.g., $Ti_{0.5}Zr_{0.25}Hf_{0.25}NiSn_{0.99}Sb_{0.01}$) having $Z_T = 1.2$ at 800 K [75].

For the inverse Heuslers, Fe_2CoGa has exhibited a negative Seebeck coefficient, low electrical resistivity, and an enhancing power factor to 400 K. Improvements have also been reported upon Co substitution [76]. Emerging quaternary Heuslers like Hf_2VZ (Z = Ga, In, Tl) show half-metallic ferromagnetism with spin-dependent thermoelectric transport—expanding applications into spin-caloritronics [77].

Despite these advances, challenges remain in further improving thermoelectric performance. The inherently high lattice thermal conductivity of the majority of Heusler compounds remains a limiting factor that demands advanced microstructural engineering like nanostructuring and grain-boundary design [78]. Synthesis of advanced Heusler phases such as quaternary or double half-Heusler systems also generally requires careful compositional control in order to attain phase purity as well as structural stability [79]. Nevertheless, continued investigation in computational materials design, experimental synthesis, and nanostructuring techniques are paving the way for the next generation of high-efficiency thermoelectric materials based on the Heusler family. Their combination of thermal stability, tunability, and eco-friendliness makes them most suitable to be integrated in energy harvesting applications, particularly industrial and automotive waste heat recovery.

1.4 Dissertation Organization

Our dissertation, is structured to provide a systematic investigation of Double half-Heusler materials, focusing on their potential for thermoelectric applications.

The **First Chapter** (Ch. 1) serves as an introduction, offering background information on thermoelectric materials, their significance, and the role of double half-Heusler compounds in energy conversion technologies.

The **Second Chapter** (Ch. 2) delves into the unique properties of double half-Heusler compounds that make them promising candidates for thermoelectric applications, discussing their structural stability, electronic configurations, and potential for high thermoelectric performance based on parameters such as the *lattice thermal conductivity*.

The **Third Chapter** (Ch. 3) introduces density functional theory (DFT), the computational framework we employ to predict and analyze the properties of double half-Heusler compounds. This chapter provides an overview of the fundamental principles of DFT, its implementation in material science, and its application in predicting structural, mechanical, electronic, thermodynamic, and thermoelectric properties.

The **Fourth Chapter** (Ch. 4) presents our results, detailing the computed properties of selected double half-Heusler compounds and analyzing their suitability for thermoelectric applications. This includes a discussion of band structures, density of states, phonon dispersion, and transport properties, with comparisons to existing experimental and theoretical data.

The **Fifth Chapter** (Ch. 5) summarizes our key findings and draws conclusions based on our results. It also discusses the broader implications of our work, potential challenges, and future research directions that could further enhance the understanding and optimization of double half-Heusler compounds for thermoelectric applications.

2

Quaternary Double half-Heusler compounds

2.1 Introduction

Quaternary Double half-Heusler compounds are an advanced class of materials that extend the traditional half-Heusler compounds by incorporating four distinct elements into their crystal structure. They are particularly interesting because they offer enhanced flexibility in tailoring properties for specific applications, such as *thermoelectrics*.

Double half-Heusler compounds have a number of *advantages* over simple *half*- or *full*-Heusler compounds in tuning their functionalities for thermoelectric applications. With the additional possibilities of a new element, the number of Double half-Heuslers is several times larger than simple Heusler compounds. Thus, they present a much larger phase space for materials discovery in comparison to the ternary compositions.

Anand *et al.* found a huge phase space of 7,719 possible quaternary half-Heusler compositions [80]. This number is over 10 times larger than that of the defect-free ternary systems (715 possible compositions) based on the same set of elements. The fraction of explored compositions for defect-free ternary systems is 64%. In stark contrast, only 0.07% of the possible quaternary half-Heusler compositions have been explored (Fig. 2.1).

2.2 Crystal Structure

Heusler compounds are closely related to Perovskites (Fig. 2.2) [81]. Inspired by Double Perovskites, in which the "Double" refer to doubling of the perovskite formula unit ($A_2B'B''O_6$ versus ABO_3), Double half-Heuslers (DhHs) can be defined as stable quaternary compounds based on *aliovalent substitution* (Overall composition is valence balanced $NV = 0$).

Quaternary compositions of the half-Heusler phases are always based on *isovalent substitution* between ternary systems without a unique valence balanced composition ($NV \neq 0$) and hence do not favor the formation of *ordered compounds* like the DhHs.

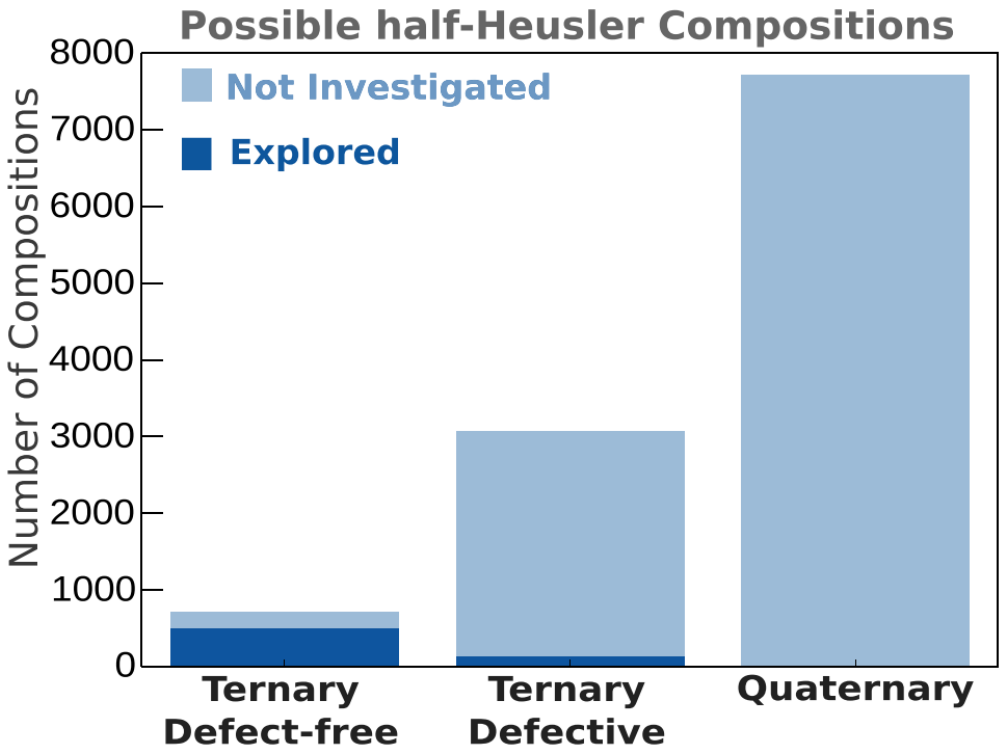

Figure 2.1: Current status of exploration in possible ternary half-Heusler systems as opposed to quaternary systems. The quaternary phase space is almost completely unexplored [80]

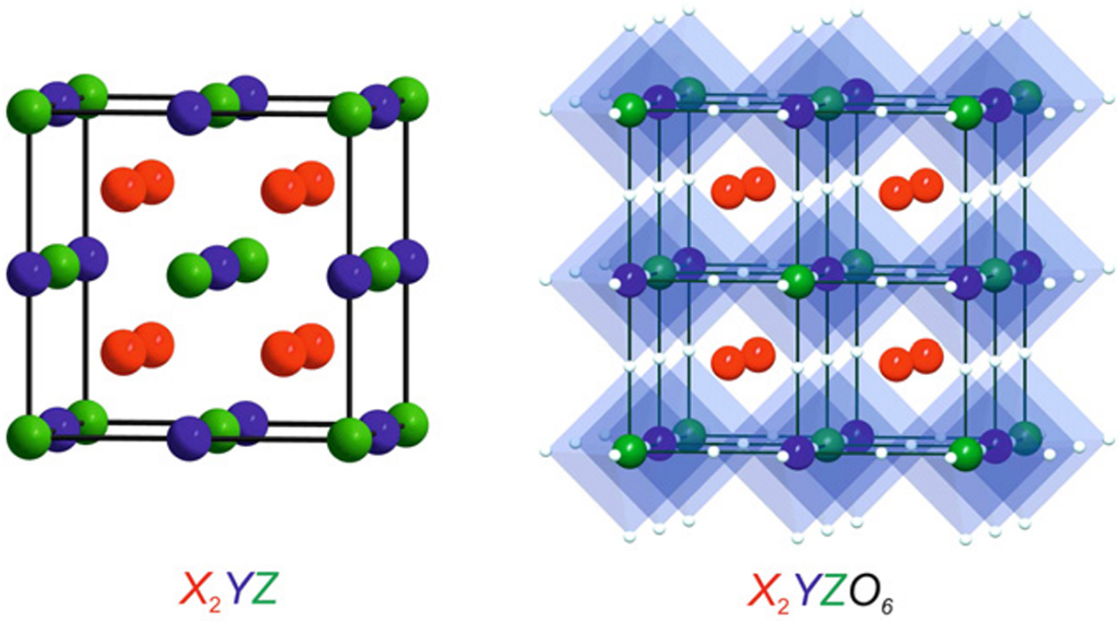

Figure 2.2: The structural similarities of Heusler compounds and Double Perovskites [81].

Double half-Heusler compounds (DhHs) crystallize in the $F\bar{4}3m$ (*Cubic*, No. **216**), $I\text{-}42d$ (*Tetragonal*, No. **122**), and $Pmn2_1$ (*Orthorhombic*, No. **31**) space groups, where the four elements occupy specific *Wyckoff positions* within the unit cell.

These compounds can be categorized into three distinct types based on the distribution of the four elements across the sublattices. The general formulas for these different classes are:

1. $XX'Y_2Z_2$: The X-sublattice is occupied by two different elements (X and X'), while the Y and Z sublattices are occupied by single elements.

   The X and X' atoms, typically transition metals or rare-earth elements, occupy the $4a$ and $4c$ sites, respectively, while the Y atom (another transition metal or rare-earth element) occupies the $4b$ site, and the Z atom (a main-group element) occupies the $4d$ site(Fig. 2.3). This ordered arrangement creates a highly symmetric structure where each atom is **tetrahedrally** coordinated by atoms of the other elements.

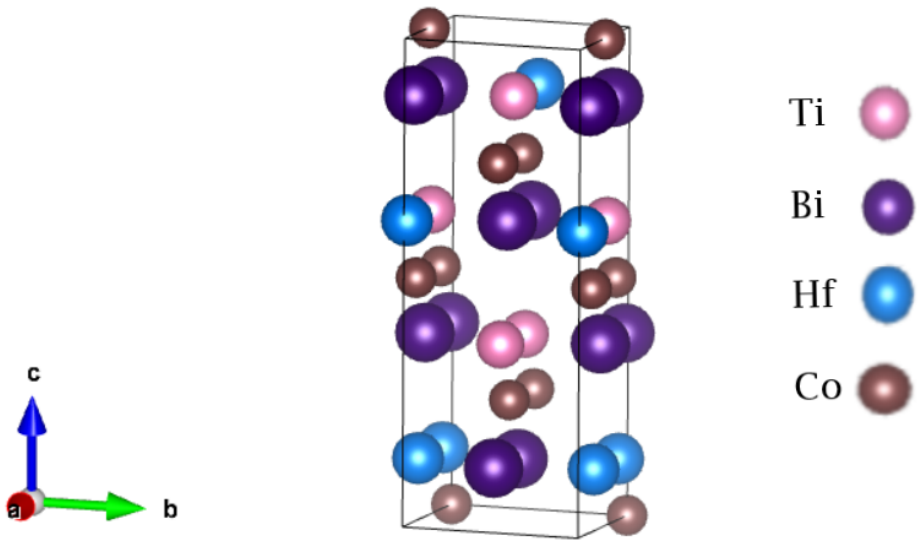

Figure 2.3: Crystal structure of $TiXCo_2Bi_2(X = Hf)$ quaternary Double Half-Heusler compounds. The pink, purple, blue, and brown spheres represent the Ti, Bi, Hf, and Co atoms, respectively.

2. $X_2YY'Z_2$: The Y-sublattice is occupied by two different elements (Y and Y'), while the X and Z sublattices are occupied by single elements(fig.2.4).

3. X_2Y_2ZZ': The Z-sublattice is occupied by two different elements (Z and Z'), while the X and Y sublattices are occupied by single elements(fig.2.5).

Depending on their classification, and according to data from the OQMD database, DhHs exhibit distinct crystallographic behaviors. Compounds belonging to the $X_2YY'Z_2$ and X_2Y_2ZZ' classes

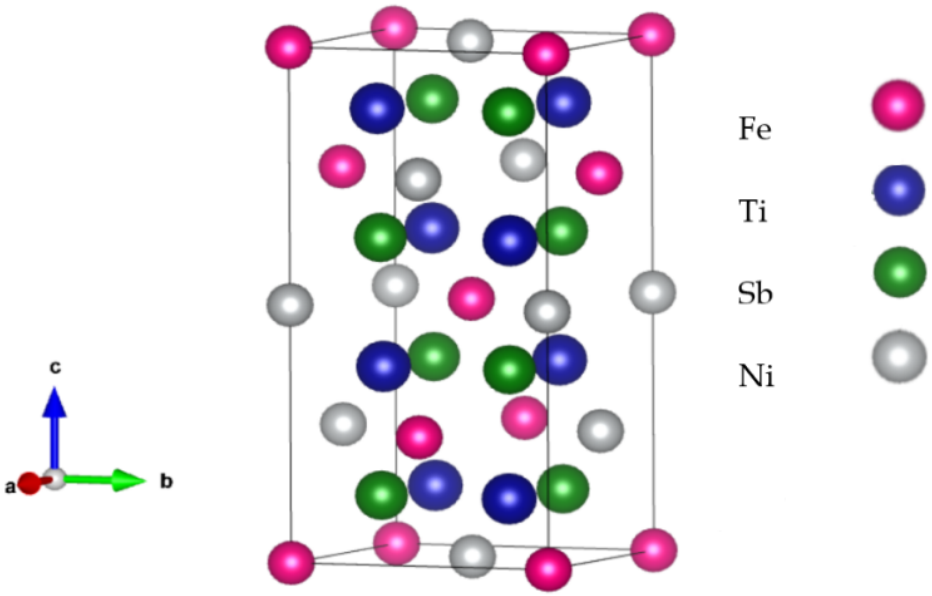

Figure 2.4: Crystal structure of $Ti_2FeNiSb_2$ quaternary Double Half-Heusler compounds. The pink, blue, green, and white spheres represent the Fe,Ti, Sb, and Ni atoms, respectively.

crystallize in the I-42d space group, whereas those in the $XX'Y_2Z_2$ class adopt the $Pmn2_1$ space group [82,83].

Experimental studies on DhHs often report a *cubic structure* ($F\bar{4}3m$ *space group*) [84], suggesting that synthesis conditions favor high-symmetry arrangements (Fig. 2.6). In contrast, theoretical investigations, particularly density functional theory (DFT) calculations, predict a **tetragonal structure**, typically in the I-42d *space group*. We think that this discrepancy arises due to factors such as atomic ordering, temperature effects, and possible distortions that are not always captured in experimental conditions but are energetically preferred in theoretical models.

Anand *et al.* found out that compounds of the $XX'Y_2Z_2$ class are predicted to be *more stable* than the other two compositions, and also *more numerous* [80]. So far, **126**, **81**, and **108** stable compounds have been predicted in the $XX'Y_2Z_2$, $X_2YY'Z_2$, and X_2Y_2ZZ' compositions, respectively.

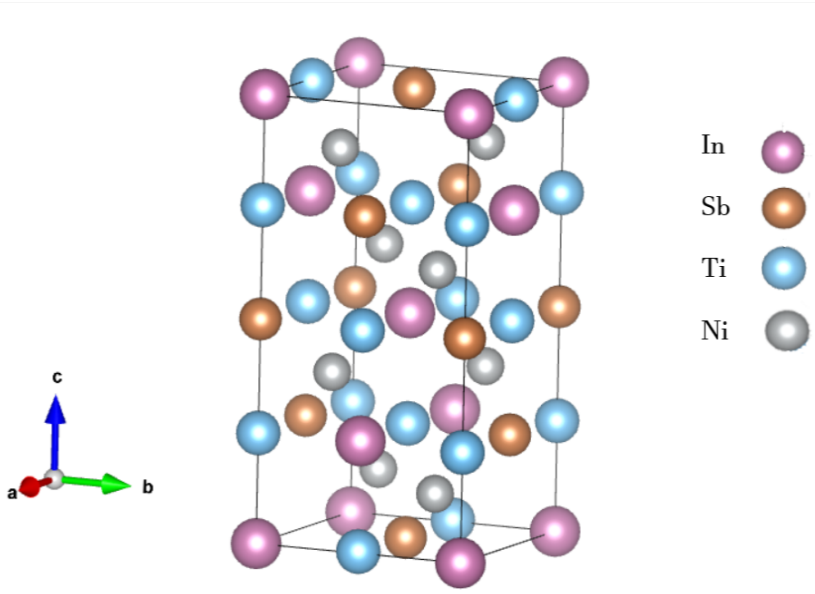

Figure 2.5: Crystal structure of Ti_2Ni_2InSb quaternary Double Half-Heusler compounds. The pink, orange, blue, and grey spheres represent the In, Sb, Ti, and Ni atoms, respectively.

Compound	*Atom*	*Wyckoff position*	x	y	z
$XX'Y_2Z_2$	X	4a	0	0	0
	X'	4b	$\frac{1}{4}$	$\frac{1}{4}$	$\frac{1}{4}$
	Y	4c	$\frac{1}{2}$	$\frac{1}{2}$	$\frac{1}{2}$
	Z	4d	$\frac{3}{4}$	$\frac{3}{4}$	$\frac{3}{4}$
$X_2YY'Z_2$	X	4a	0	0	0
	Y	4b	$\frac{1}{2}$	$\frac{1}{2}$	$\frac{1}{2}$
	Y'	4c	$\frac{1}{4}$	$\frac{1}{4}$	$\frac{1}{4}$
	Z	4d	$\frac{3}{4}$	$\frac{3}{4}$	$\frac{3}{4}$
X_2Y_2ZZ'	X	4a	0	0	0
	Y	4b	$\frac{1}{2}$	$\frac{1}{2}$	$\frac{1}{2}$
	Z	4c	$\frac{1}{4}$	$\frac{1}{4}$	$\frac{1}{4}$
	Z'	4d	$\frac{3}{4}$	$\frac{3}{4}$	$\frac{3}{4}$

Table 2.1: Wyckoff positions and atomic coordinates for quaternary double half-Heusler compounds

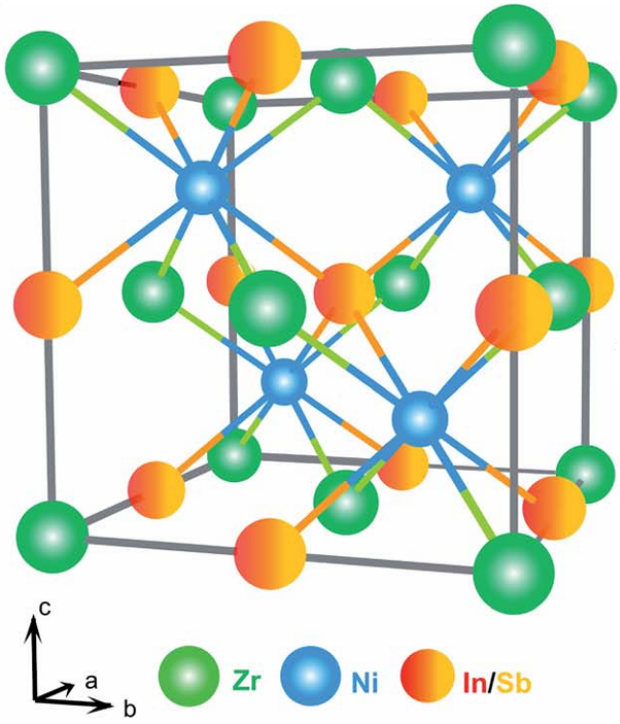

Figure 2.6: Unit cell of the cubic crystal structure of ZrNi (In, Sb) double half-Heusler compound.

Class	*Space group*	*Compounds*	*Ref.*
$XX'Y_2Z_2$	$Pmn2_1$	$ScXCo_2Sb_2$ (X = V, Nb, Ta)	[85]
		$TiXCo_2Bi_2$ (X = Zr, Hf)	[86]
		$ZrHfCo_2Bi_2$	[86]
		$LuXCo_2Sb_2$ (X = V, Nb, Ta)	[87]
		$LuXNi_2Sn_2$ (X = V, Nb, Ta)	[88]
		$MgXY_2Z_2$ (X = Zr/Hf, Y = Pd/Pt, Z = Bi/Sb)	[89]
$X_2YY'Z_2$	$I\text{-}42d$	$Ti_2FeNiSb_2$	[90]
		$Nb_2FeNiSn_2$	[91]
		$Ta_2FeNiSn_2$	[91]
		$X_2FeY'Sb_2$ (X = Hf, Zr; Y' = Ni, Pd)	[92]
		$M_2FeNiSb_2$ (M = Ti, Hf)	[93]
		$Mn_2FeCoSi_2$	[94]
		Mn_2CoCrZ_2 (Z = P, As)	[95]
		Zr_2XBiNi_2 (X = Al, Ga)	[96]
X_2Y_2ZZ'	$I\text{-}42d$	Ti_2Ni_2InSb	[90]
		Zr_2Ni_2InSb	[97]

Table 2.2: Classification of Quaternary Double half-Heusler Compounds according to their structural class.

2.2.1 Structure-Property Relationships

The structural complexity of QDHHs enables precise control over their electronic, magnetic, thermal, and mechanical properties, making them highly attractive for a wide range of applications.

- Electronic Properties:

  QDHH compounds possess a highly tunable electronic band structure due to the incorporation of four distenct elements, allowing fine-tuning of the band gap and density of states. This tunability is essential to optimize electrical conductivity and semiconducting characteristics, particularly in thermoelectric applications [98]. For instance, compounds such as (Zr,Ni)InSb have demonstrated enhanced thermoelectric properties owing to their optimized electronic properties and precise compositional tuning (e.g., Co and Hf doping), which balance high electrical conductivity(fig. 2.7) with low thermal conductivity and can enrich the HH family by enabling the identification of novel materials [99].

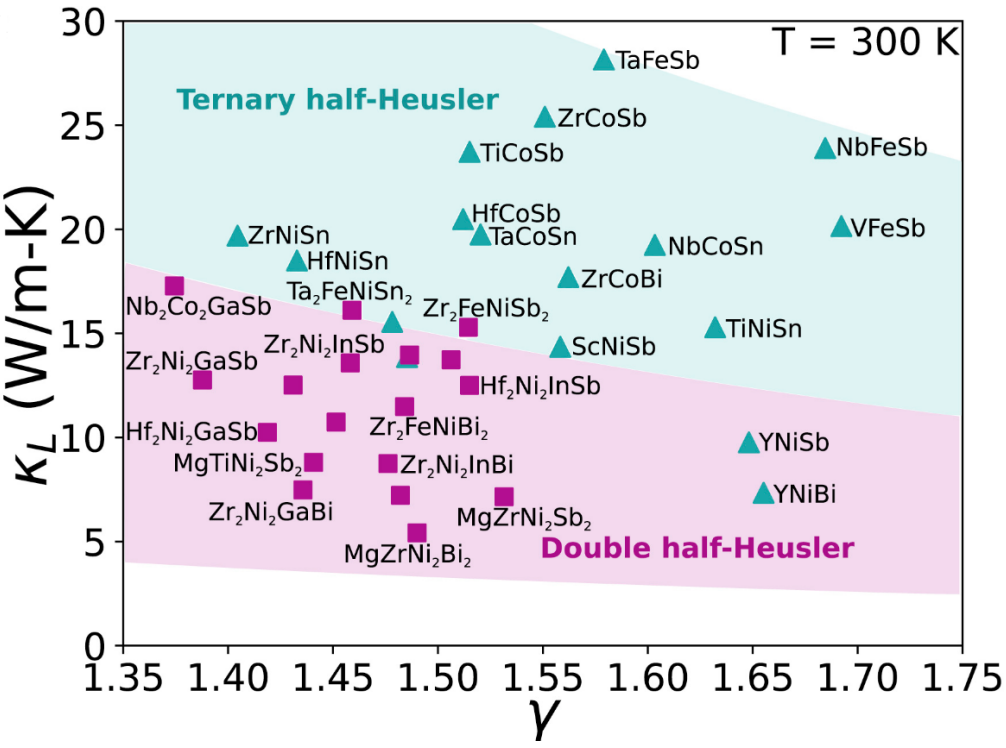

Figure 2.7: Lattice Thermal Conductivity Comparison of Double Half-Heusler and Corresponding Ternary Half-Heusler [80].

In addition, their ability to engineer the band structure also makes these materials promising candidates for next-generation electronics and optoelectronics. [90].

- Magnetic Properties:

  The magnetic nature of QDHH compounds is strongly dependent on the relative ordering and nature of the magnetic ions in the structure. Transition metal bearing compounds like

Mn, Fe, or Co may be antiferromagnetic, ferromagnetic, or even nonmagnetic based on atomic composition and ordering.[100]. Some of these materials, such as those with high spin polarization, are being explored for spintronic applications, where the manipulation of electron spin can lead to more efficient data storage and processing technologies. Furthermore, certain compositions exhibit magnetocaloric effects, making them suitable for magnetic refrigeration systems[101, 102].

- Thermal Properties:

  One of the most important features of QDHH compounds is their low thermal conductivity which arises from increased phonon scattering from their complex crystal structures. It is a particularly desired feature in thermoelectric applications, where minimizing thermal conductivity while maintaining high electrical conductivity is essential fo obtaining high thermoelectric efficiency. Compounds such as $(Ti, Zr, Hf)NiSn$[103] have shown very good thermoelectric properties with high Z_{T} values at high temperature and are therefore well suited for power generation and waste heat recovery applications[80] [104].

- Mechanical Properties:

  The mechanical properties of these compounds, including hardness and elasticity, are affected by the bonding nature between the elements involved. Strong covalent bonding has a tendency to impart high hardness, but the complex structure can also render it brittle. However, careful choice of the elements and advanced processing techniques, such as spark plasma sintering (SPS), can reduce these issues and improve mechanical strength. Such properties are important to provide the structural integrity of materials used in high-stress or high-temperature applications[105].

2.3 Stability

2.3.1 Structural stability:

The structural stability of quaternary double half-Heusler (QDHH) compounds is essential for preserving their ordered crystal structure under varying thermal and pressure conditions[106] [107]. These materials consist of two interpenetrating half-Heusler units, resulting in a larger unit cell and increased complexity. Their stability is primarily influenced by bonding strength and hybridization (e.g., strong d–d hybridization in TiZrCoIn-Ge enhances stability)[52, 108], lattice symmetry and atomic ordering[109, 110], and defect formation energies[111, 112].

Atomic site occupancy is shaped by factors such as atomic radii, similar sizes (e.g., Hf: 159 pm, Zr: 160 pm) reduce strain and enhance stability, while mismatches (e.g., V: 134 pm vs. Nb: 145 pm) can cause lattice distortion and phase separation if not controlled[113–115]). Electronegativity affects bonding types, Fermi level position, and DOS[11], while a balanced mix of ionic, covalent,

and metallic bonding (from elements like Ti, Co, Sb, and Sn) improves mechanical and electronic properties [116–118]. Stable QDHH compounds generally show low formation enthalpy (ΔHf) [119], high cohesive energy [120], criteria [121].

Cohesive energy E_{coh} is calculated as:

$$E_{\text{coh}} = \frac{E_{\text{isolated atoms}} - E_{\text{solid}}}{N} \tag{2.2}$$

Where:

- $E_{\text{isolated atoms}}$ is the total energy of the isolated atoms in the system.
- E_{solid} is the total energy of the solid.
- N is the number of atoms in the solid.

Lattice parameter matching further reduces internal stress. Nonetheless, antisite defects and atomic disorder can disrupt structural integrity, necessitating controlled synthesis and compositional tuning to ensure stability.

2.3.2 Thermodynamic Stability:

Thermodynamic stability in QDHH compounds is primarily determined by a negative formation energy calculated via Density Functional Theory):

$$\Delta H_f = E_{\text{compound}} - \sum_i n_i E_i \tag{2.4}$$

where:

- E_{compound} is the total energy of the QDHH compound.
- E_{i} is the total energy of element i in its standard state (bulk or isolated state).
- n_{i} is the number of atoms of element i in the compound.

It is essential for their synthesis and practical use. A compound's proximity to the convex hull determines its stability under equilibrium conditions—those on or near the hull are more likely to be stable and synthesizable [122].

However, quaternary systems often face decomposition due to competing binary or ternary phases, requiring careful compositional tuning. For example, DFT calculations show that compounds like $Ti_2FeNiSb_2$ lie near the convex hull, indicating potential thermodynamic stability [98]. At high temperatures ($\sim$ 1000 K), entropic contributions can further favor the formation of these phases [123].

While high configurational entropy may help stabilize disordered quaternary structures, ordered QDHH phases demand precise stoichiometry. Deviations can lead to decomposition into full-Heusler (e.g., Co_2TiSi), half-Heusler (e.g., $TiCoSb$), or simpler binary phases (e.g., Mg_2Sb, $TiNiSn$). Thus, achieving QDHH stability requires balancing formation enthalpy, entropy, and phase competition to maintain the desired crystal structure.

2.4 Synthesis techniques/Past experimental reports

Double half-Heusler compounds typically are synthesized by a combination of arc melting, ball milling, hot pressing or SPS, and annealing at high temperatures [80, 84, 124]. Arc melting in an inert argon atmosphere allows for effective mixing of stoichiometric amounts of high-purity elemental precursors. For instance, Shi et al. used arc melting followed by subsequent SPS to synthesize $Ti_2NiZrSb_2$ and $Ti_2NiHfSb_2$ compounds, up to Z_T of 0.9 at 800 K [125]. The ingots were flipped and remelted multiple times to ensure compositional homogeneity, then ground into powders to enhance surface area and facilitate densification.

These powders are often subjected to ball milling to customize particle size and reactivity. The resulting consolidation is performed using hot pressing or SPS, involving uniaxial pressure and heating to create dense polycrystalline pellets of low porosity. In the case of $Ti_2FeNiSb_2$, by Gofryk et al. Arc melting followed by prolonged annealing was employed to obtain a disordered $C1_b$-type half-Heusler phase, in which atomic disorder at the X site was found to enhance phonon scattering and thus the efficiency of thermoelectricity [126].

Annealing at 800 and 1000 °C temperatures is a critical step to improve crystallinity, eliminate internal stress, and stabilize the desired half-Heusler phase. Zhang et al. synthesized $Ti_2NiCoSb_2$ by arc melting and annealing, confirming phase purity and ensuring phase purity and recording enhanced Seebeck coefficients attributed to favorable carrier concentration tuning [127].

Aside from conventional synthesis methods, innovative methods such as SPS and melt spinning have been employed to achieve nanostructured DHH materials. This method produces rapidly quenched ribbons , which are sintered and pulverized, enhancing phonon scattering and reducing lattice thermal conductivity. Although effective, the method is less adopted due to its complexity.

Despite these developments, experimental investigation of DHH materials remains relatively limited. Several theoretically predicted compounds, such as $Ti_2OsNiSb_2$, $Ti_2OsPdSb_2$, and $Ti_2OsPtSb_2$, have not yet been synthesized, largely due to the cost and toxicology of osmium-based components [128]. Computational predictions, nevertheless, indicate that such compounds would exhibit excellent thermoelectric performance, motivating continued experimental efforts.

2.5 Potential for Thermoelectricity

Traditional half-Heusler compounds with cubic symmetry (space group $Fm\bar{4}3m$) exhibit high electrical conductivity due to efficient carrier transport through three interpenetrating FCC sublattices. However, their ordered structure promotes rapid phonon propagation, resulting in high lattice thermal conductivity (κ_L) and limited thermoelectric performance.

Double half-Heusler compounds overcome this by introducing structural complexity, such as unit cell doubling, atomic layering, or interstitial atoms, which lowers symmetry (e.g., orthorhombic or tetragonal phases) and introduces atomic disorder, vacancies, and heterogeneous bonding. These changes scatter phonons and reduce κ_L, while simultaneously increasing the density of states and promoting band degeneracy, which enhances the Seebeck coefficient and power factor .

For instance, in $TiFe_{1.5}Sb$, delocalized d-states support high conductivity ($\sim 10^5$ S/m), while covalent-metallic networks preserve carrier mobility. Despite high conductivity, DHHC maintain large Seebeck coefficients (200–300 $\mu V/K$) due to band convergence and enhanced DOS, achieving power factors $\sim 50\%$ higher than those of HHCs [129].

Thermal conductivity is also significantly reduced (e.g., from 5-8 W/mK in HHCs to 2-3 W/mK in DHHCs) through mass contrast, hierarchical defects, and multi-scale phonon scattering. As a result, DHHCs such as ZrCoBi have reached figures of merit > 1.5 at 900 K [130], with some approaching 2.0-2.5, nearly double that of traditional HHCs (fig.2.8).

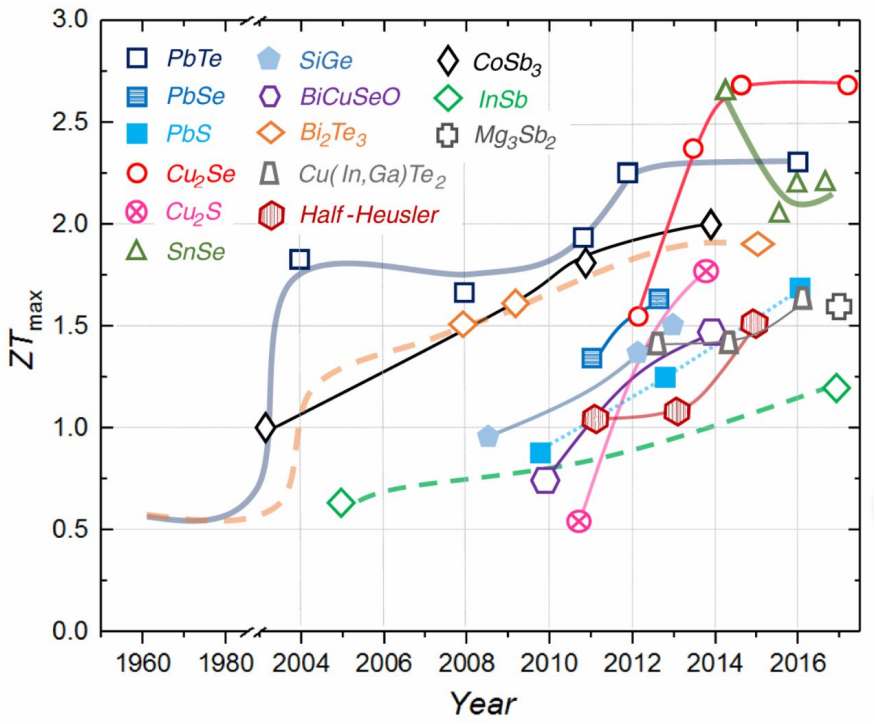

Figure 2.8: Timeline of the maximum ZT values for several representative families of TE materials. Review of a number of promising TE materials, among which are half-Heuslers compounds [131].

Despite these advantages, challenges remain in synthesis and scalability. Techniques like spark plasma sintering or melt-spinning are often required, and excessive defect engineering may harm electrical transport. Furthermore, peak performance is limited to specific systems (e.g., Ti/Zr/Co-based), emphasizing the need for careful doping and microstructure control.

2.6 Computationally guided discovery of thermoelectric materials

Computations are transitioning from providing retrospective explanations of experimental results to giving guidance for the exploration of promising materials.

High-throughput searches will narrow down the search space to the most promising materials classes; this information will then be used to identify promising materials and perform calculations of greater accuracy within a narrower search space.

Several large databases of first-principles calculations have emerged, including **Materials Project** [132], **AFLOWLIB**, **OQMD** [82, 83], and **TEDesignLab**.

2.6.1 High-throughput computational searches (Inverse design)

What we often really would like to have is an inverse approach to material design (inverse design), in which the desired target properties are used as input to predict the materials that exhibits them.

Here, a new style of collaboration between theory and experiment is discussed, whereby the desired functionality of the new material is declared first and theoretical calculations are then used to predict which stable and synthesizable compounds exhibit the required functionality.

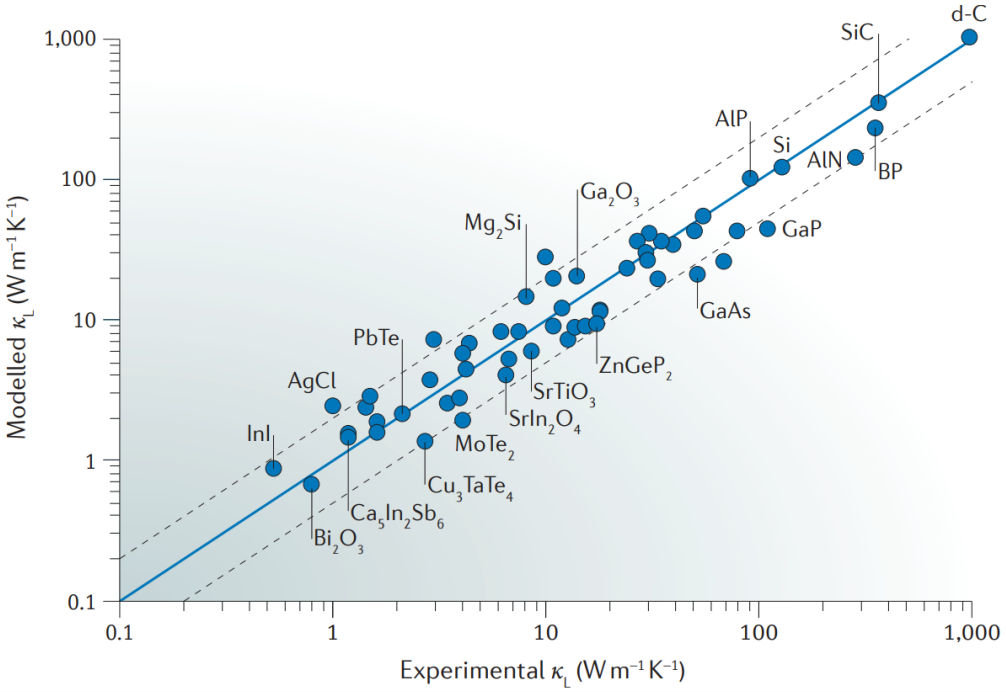

Figure 2.9: Values for κ_L predicted with a *semi-empirical model* are compared with the experimental values [133].

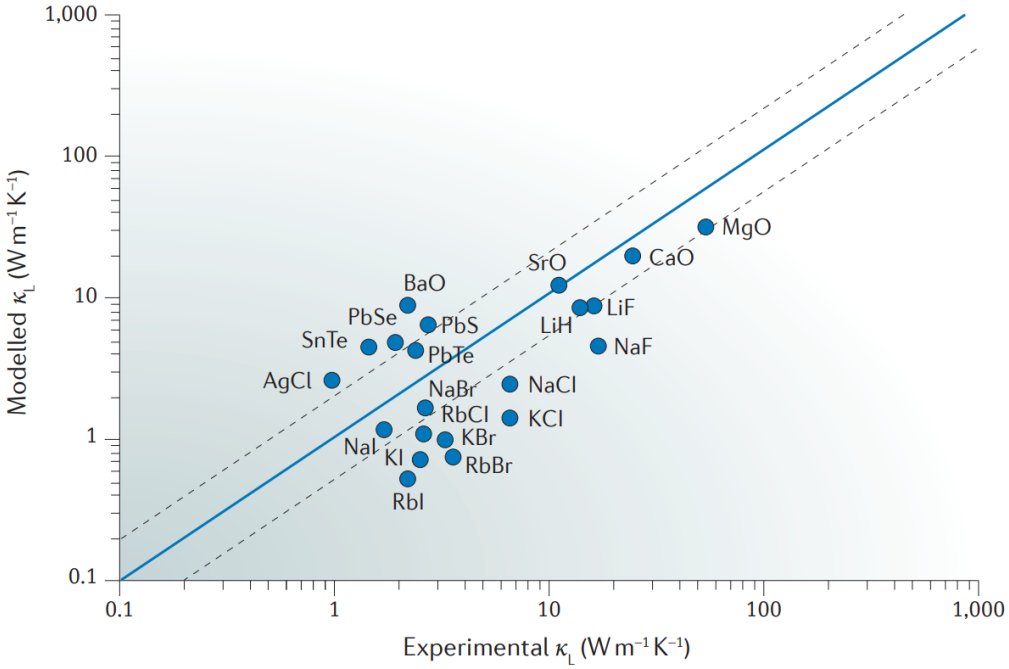

Figure 2.10: Values for κ_L predicted with a *quasi-harmonic Debye model* are compared with the experimental values [133].

Figures $\sim$ 2.9, 2.10, and 2.11 present the predicted values of lattice thermal conductivity (k_{L}) obtained from high-throughput models, including the semi-empirical approach, the quasi-harmonic Debye model, and the Slack model, in comparison with experimental data.

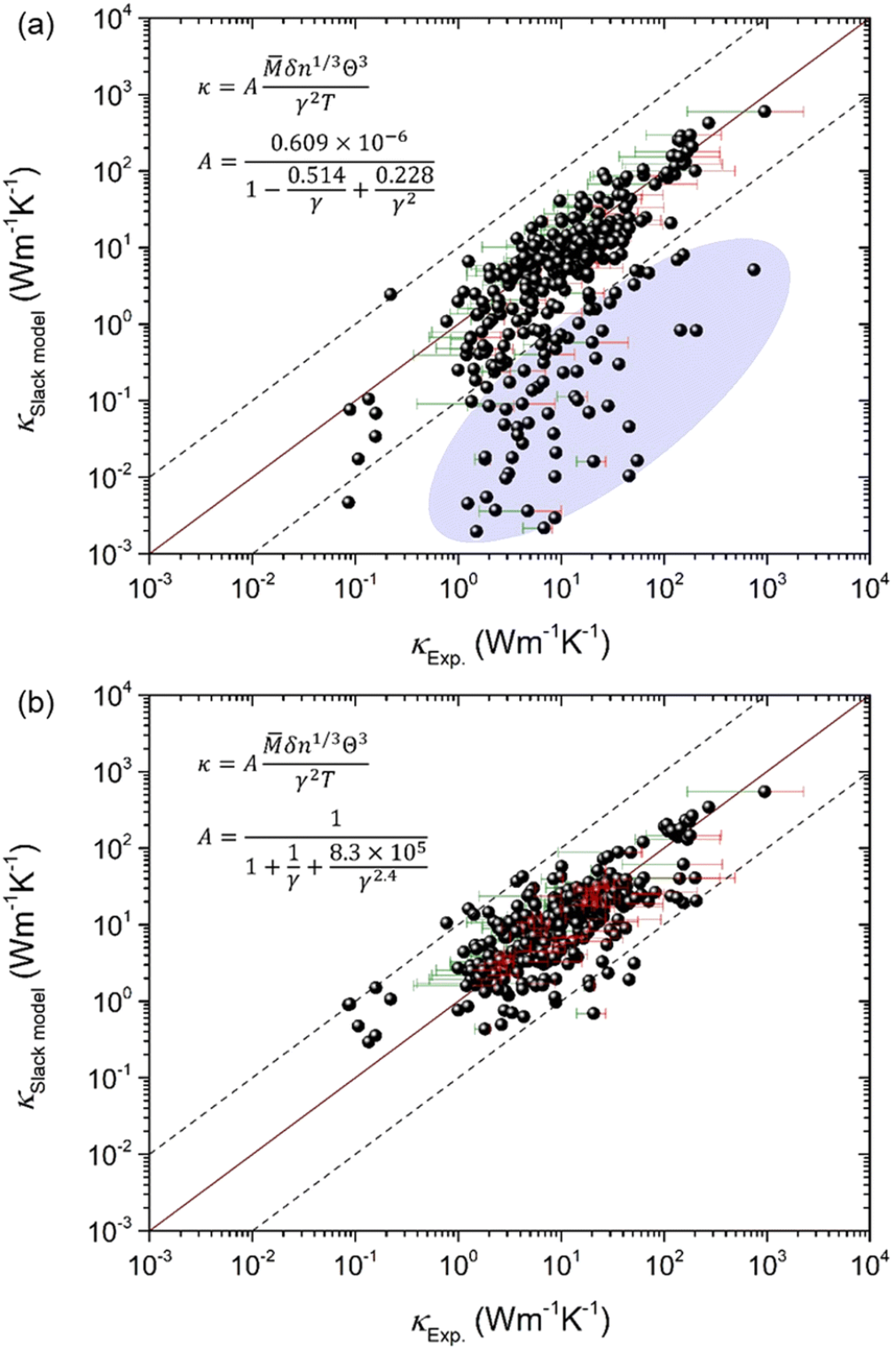

Figure 2.11: Comparison between the lattice thermal conductivity κ_L calculated by the *Slack model* and the κ_L measured in experiments (κ_{exp}), for a large set of 353 materials. [134]

2.6.2 Detailed single-candidate calculations (Direct design)

The conventional approach to the discovery of materials with target properties generally involves studying experimentally and explaining theoretically the properties of a given material. Using this so-called direct approach involves the use of the three descriptors of a material (atomic identities, composition and structure) as input to derive the ensuing material properties.

This approach enables the identification of previously known materials with hitherto unrecognized (or not measured) properties from a database of known compounds.

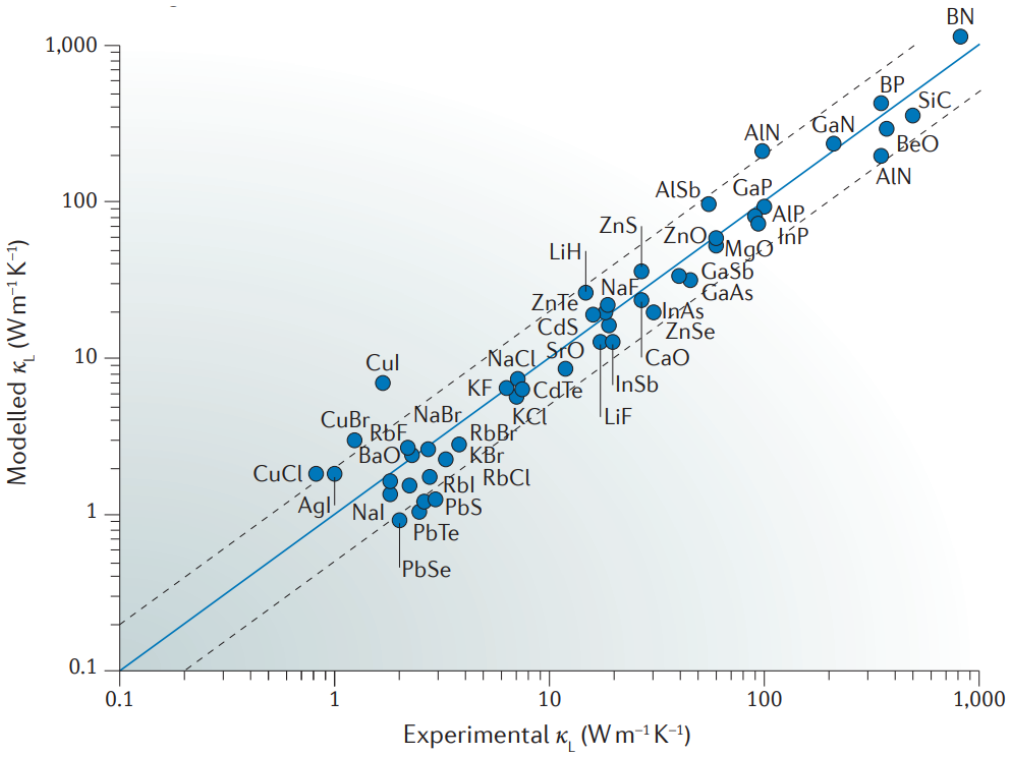

Figure 2.12: Values for κ_L predicted using rigorous *third-order force constants* are compared with the experimental values [133].

Figure ∼ 2.12 shows the k_{L} values predicted using third-order force constants, demonstrating high agreement with experimental measurements and highlighting the strength of direct design approaches.

3

Density Functional Theory (DFT) Calculations

Materials modeling and design using computational quantum and classical approaches is by now well established as an essential pillar in condensed matter physics, chemistry, and materials science research. Simulations can greatly accelerate the identification, characterization, and optimization of materials.

Because of its relatively high predictive power, versatility, and computational efficiency, DFT is currently the method of choice to compute efficiently and often accurately the ground-state properties of condensed systems: these include the energy of the ground state and its derivatives (for example, forces and stresses, that are used to find equilibrium structures). It is a widely used and mature technology.

3.1 What is density functional theory? (Introduction to DFT)

Density Functional Theory (DFT) is an approach to study the behavior of electrons in materials. It recasts the complicated Schrödinger equation (which describes the motion of electrons) in a form that is more readily solvable for actual materials. Introduced in **1964** by Hohenberg and Kohn, the theory showed that all the important properties of a material can be described using just the electron density (which describes where electrons are likely to be). They proved that you can find the lowest energy of a system by adjusting this density. Such an approach involves iteratively refining an initial guess of the electron density instead of solving the full Schrödinger equation directly. Later, Kohn and Sham made the theory applicable in practice by rewriting the equations to isolate the complex electron-electron interactions into what is known as the exchange-correlation functional. While the exact form of this functional remains unknown, effective approximations based on how electrons behave in simple systems, like an electron gas and further extensions have proven to be successful for a wide range of materials.

The accuracy of a DFT calculation depends largely on the choice of the exchange-correlation functional. Although more sophisticated functionals can enhance accuracy (often at increased computational cost), they frequently fail for highly correlated electron systems. Standard DFT also

has several other limitations, it can typically handle only relatively small systems (currently available computational powers tend to treat periodic unit cells with approximately 1,000 or fewer atoms). Additionally, it has difficulty accurately modeling weak interactions (e.g., van der Waals forces), long-time behavior, and non-ground-state phenomena, e.g., finite-temperature effects or electronic excitations. Fortunately, various techniques have been developed to address these challenges. For instance, linear scaling methods facilitate simulation of larger systems; lattice dynamics and cluster expansion methods enable finite-temperature effects, and techniques such as time-dependent DFT, the GW approximation, and Bethe–Salpeter equation account for excited-state properties. Van der Waals interactions can also be handled better by empirical corrections or non-local functionals. Thus while DFT has inherent limitations, methodological advances still extend its applicability.

To perform a DFT calculation, you need to provide some inputs: the material's atom types and positions in the periodic lattice, exchange-correlation functional option, and a few convergence-controlling parameters and algorithms, together with some numerical iterative controls. Optionally, a method such as pseudopotentials may be employed to more efficiently handle core electrons. Calculation outputs fundamental electronic properties such as the charge density, total energy, magnetic ordering, and band structure. However, to obtain useful, real-world properties from these calculations, further analysis is generally needed.

In recent decades, the application of DFT techniques for interpreting and predicting material properties has expanded rapidly. This growth is driven by the development of user-friendly software tools (both commercial and open-source), improved and more efficient algorithms for solving DFT equations, and the widespread availability of affordable computing power. Nowadays, large materials databases containing the outcomes of tens or even hundreds of thousands of DFT calculations are publicly accessible, making these results available to both theoretical and experimental researchers.

3.2 Outputs of a DFT computation

The output of the density functional theory (DFT) calculation yields fundamental quantities such as the electron charge density $\rho(\mathbf{r})$ which is one of the key DFT outputs providing information on the spatial distribution of electrons in a system. Since the Hohenberg-Kohn theorem demonstrates that all ground-state properties are expressed by the charge density, this parameter plays a crucial role in the description of chemical bonding, charge transfer, and electronic localization. By analysis of $\rho(\mathbf{r})$, researchers can identify covalent, ionic, and metallic bonds, chart electron gain or loss in bonding areas, and explore charge redistribution as a function of external perturbations (e.g., adsorption or catalysis). The electron density difference calculated from the total density minus the atomic densities is also helpful for unmasking how electrons redistribute upon bond formation. Another DFT output is the total energy which is equal to the ground-state energy of the entire system,

including the electron kinetic energy, electron-electron repulsion, electron-nuclei attraction, and nuclei-nuclei repulsion. It is derived from the Kohn-Sham equations solution and It is a significant parameter in determining the thermodynamic stability of a structure. The general DFT workflow, starting from an input crystal structure to the calculation of electronic properties such as band structure and density of states, is illustrated in (fig.3.1). Total energy comparisons allow researchers to compare the relative stability of different phases, defect configurations, or surfaces and to estimate formation and cohesive energies. also the DFT enables geometry optimization by relaxing both lattice parameters and atomic positions to locate the total energy minimum of a system. This locates the most stable (lowest energy) structure, a local minimum on the potential energy surface, and is the most physically realistic atom arrangement. Optimized geometries are needed to predict equilibrium structures, particularly in cases where the experimental data are limited , e.g., metastable compounds or high-pressure phases. Elastic constants and bulk modulus can be extracted from the optimized geometries obtained, thermal expansion can be determined, or defect formations can be investigated.

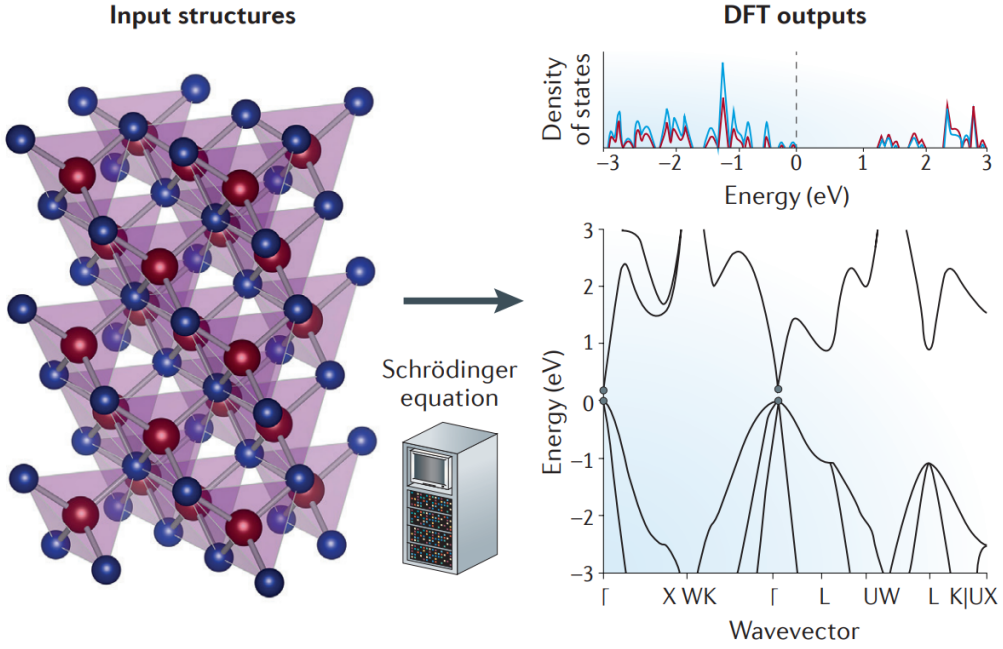

Figure 3.1: The DFT calculations require, as an input, a reasonable estimate of the crystal structure. The output of the calculations yields fundamental quantities such as the electron charge density, total energy, optimized crystal structure and band structure.

For molecular systems, DFT optimizations yield bond lengths, angles, and conformations, information about reaction mechanism, and intermolecular interaction. in addition to that, Band structure, as obtained from Kohn-Sham eigenvalues in Density Functional Theory (DFT), describes the relationship between electron energy levels and crystal momentum in a solid, which dictates whether a material is a metal, semiconductor, or an insulator. It provides valuable insights into the nature and width

of the band gap, significant charge carrier effective masses, and potential topological or spin-orbit effects, and informs predictions of transport and optical properties. Since conventional standard DFT approaches like LDA and GGA have a tendency to underestimate band gaps, more advanced methods like hybrid functionals or GW corrections are typically used to enhance reliability.

3.3 DFT advantages over experimental procedures

Density Functional Theory (DFT) offers several advantages over experimental procedures:

1. **Cost-Effective:**
   - No need for expensive equipment or materials.
   - Reduces the cost of trial-and-error in material synthesis.
2. **Time-Saving**
   - Can quickly screen a wide range of materials or properties.
   - Eliminates time-consuming sample preparation and testing.
3. **Atomic-Level Insight**
   - Provides detailed information about electronic structure, bonding, charge density, etc.
   - Helps in understanding phenomena not directly accessible by experiments.
4. **Controlled Environment:** Simulations can be run under idealized or extreme conditions (high pressure, temperature, vacuum, etc.) that may be difficult to achieve experimentally.
5. **Prediction of Properties**
   - Can predict properties (e.g., mechanical, electronic, optical, thermodynamic) of unknown compounds (materials that have not yet been synthesized) 3.2, 3.3.
   - Useful for designing new materials.
6. **Complement to Experiment**
   - Can help interpret experimental data and explain trends.
   - Allows separation of individual contributions (e.g., electronic vs. ionic) to properties.
7. **No Material Constraints:** Useful when materials are toxic, unstable, radioactive, or very rare, making experiments dangerous or impractical.

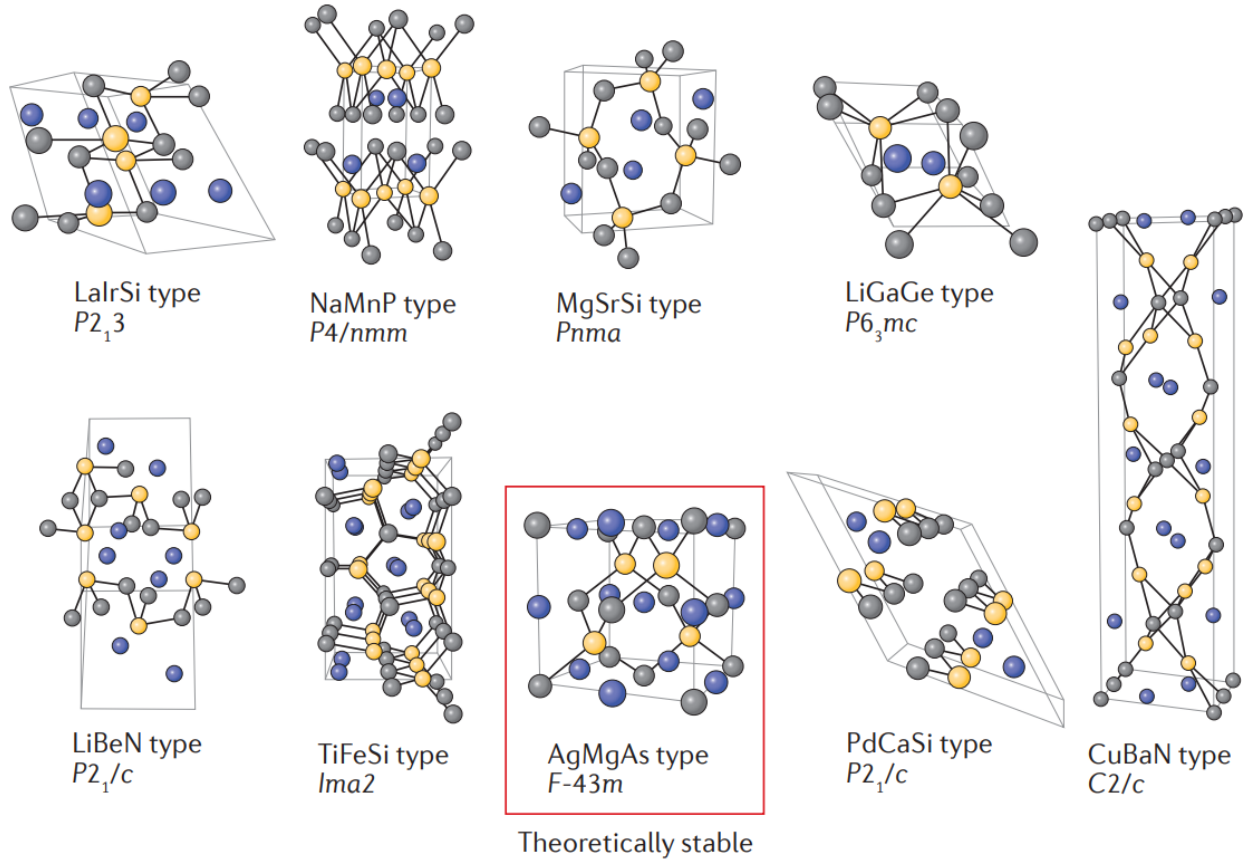

Figure 3.2: Potential ABX crystal structures for TaIrGe [135].

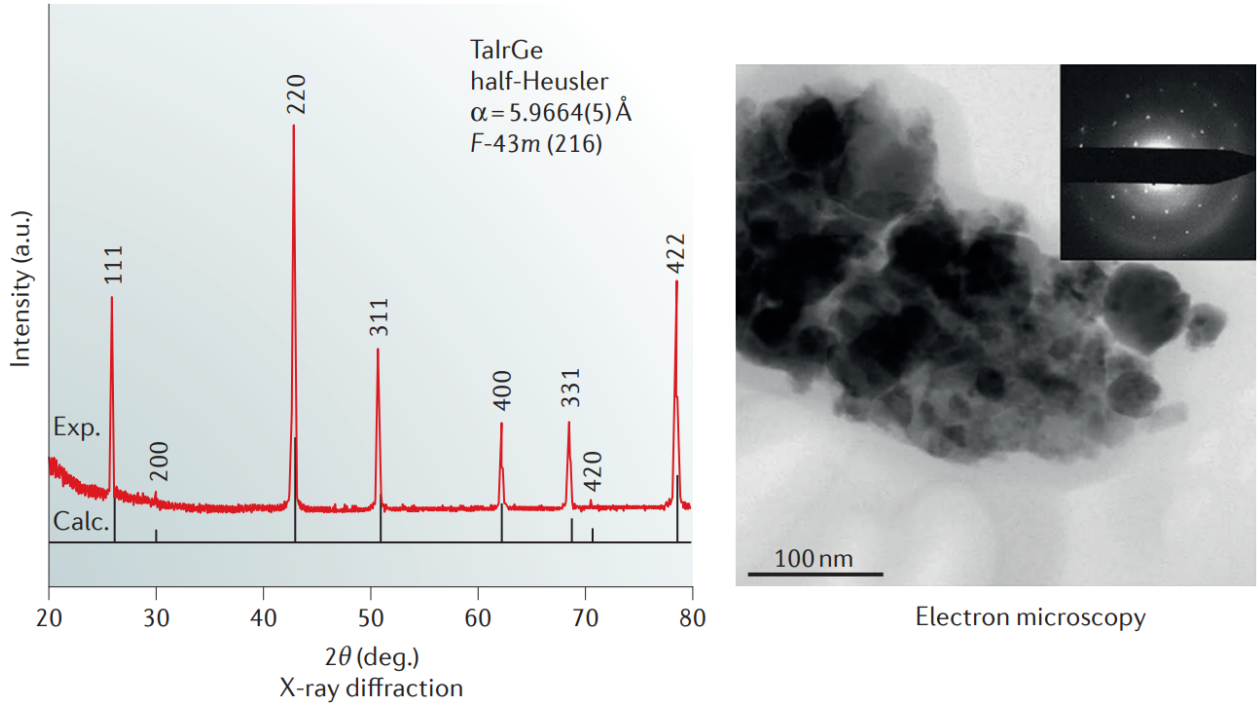

Figure 3.3: Experimental confirmation of the predicted crystal structure [135].

3.4 DFT for thermoelectrics

Density Functional Theory (DFT) is an extremely valuable resource for the design and development of thermoelectric materials, as it provides atomistic data on their electronic and vibration behavior. Thermoelectric performance is commonly defined in terms of the dimensionless figure of merit $z_{\mathrm{T}} = \frac{S^2\sigma T}{\kappa_l}$ [136]. Using electronic band structure simulation, DOS, and carrier effective mass simulation, DFT can predict critical parameters such as the power factor $S^2\sigma$, which defines thermoelectric performance.

When combined with semi-classical transport theories such as the Boltzmann Transport Equation, often implemented through software like BoltzTraP, DFT enables the calculation of temperature-dependent transport properties, including the Seebeck coefficient, electrical and thermal conductivity [137]. This allows for performance prediction across a variety of conditions, reducing the need for large scale experimental synthesis.

This integrated approach significantly accelerates the pre-experimental design and supports the exploration of strategies such as band convergence, defect engineering, and nanostructuring to enhance electrical transport while suppressing thermal losses. To further process the lattice thermal conductivity (the central factor in maintaining a temperature gradient), DFT is generally supplemented by Density Functional Perturbation Theory (DFPT), which enables the computation of the dispersion and lifetime of the phonon, providing deeper insights into lattice dynamics and phonon scattering mechanisms [138]. Such information informs approaches like nanostructuring and alloying to effectively reduce thermal conductivity.

DFT has played a core role in discovering and optimizing high-performance thermoelectric materials like Bi_2Te_3, SnSe, and half-Heusler compounds. While complicated scattering mechanisms (e.g., electron–phonon and phonon–phonon interactions) remain challenging to model accurately. Recent advances, particularly the integration of DFT with machine learning techniques are expanding prediction capabilities and ever more accelerating materials innovation.

3.5 Quantum ESPRESSO

Quantum ESPRESSO (Quantum opEn-Source Package for Research in Electronic Structure, Simulation, and Optimization) is an open-source suite of computer codes for electronic-structure calculations and materials modeling, Developed by global collaborative efforts from scientists and institutions. It was built on Density Functional Theory (DFT), pseudopotentials, and plane-wave basis sets to allow scientists to investigate an array of material's physical and chemical properties such as total energy, atomic forces, vibrational modes, and electronic band structures at the quantum mechanical level.

It is essential to prepare an input file for the pw.x module in order to perform a calculation in

Quantum ESPRESSO, which must include key informations such as:

- The type and control of the calculation are set in the `&CONTROL` namelist using variables such as `calculation`, `prefix`, `outdir`, and `pseudo_dir`.
- The plane-wave cut-off energies specified in the `&SYSTEM` namelist using `ecutwfc` for the wavefunction and optionally `ecutrho` for the charge density, along with the smearing parameters defined by `occupations`, `smearing`, and `degauss`.
- The electronic self-consistency parameters are defined in the `&ELECTRONS` namelist, including `conv_thr` for the SCF convergence threshold and `mixing_beta` for charge mixing control.
- The types of atoms and their corresponding pseudopotential files are defined under the `ATOMIC_SPECIES` section, including atomic masses and pseudopotential filenames.
- The atomic positions within the unit cell are specified in the `ATOMIC_POSITIONS` section using either fractional (`crystal`) or Cartesian (`angstrom`) coordinates.
- The k-point mesh used for Brillouin zone integration is specified in the `K_POINTS automatic` section.

3.5.1 Precision compared to other DFT implementations (Codes)

QE is renowned for its accuracy, versatility, and utility in solid-state and materials simulations. Its plane-wave basis set produces systematic and controlled convergence with accurate reliability for a wide class of materials without the widespread errors associated with localized basis sets, e.g., in codes such as Gaussian or ORCA. QE facilitates a wide range of high-quality pseudopotentials such as norm-conserving, ultrasoft, and PAW from well-tested libraries such as PSlibrary and SSSP that allow for the efficient and precise modeling of both light and heavy elements with higher flexibility and number of pseudopotentials than others such as ABINIT, rendering it suitable for bulk solids, surfaces, and interfaces.

The code supports broad exchange-correlation functional ranges from LDA to GGA, meta-GGA, and hybrid functionals such as PBE0 and HSE, supporting a range of applications from bandgap calculation to highly correlated systems. The code is on par with commercial programs such as VASP in terms of accuracy and functionality, including hybrid functionals and van der Waals corrections, with the additional benefit of being entirely open-source and heavily customizable. Its modularity comprises state-of-the-art features like spin-orbit coupling and linear-response theory, and offers interfaces to external tools like Wannier90, EPW, and Yambo for post-DFT calculations, including excited-state properties and GW, with a robust ecosystem that rivals both open-source and commercial ones.

With faster convergence, good parallelism performance, and an open development community, QE has an excellent accuracy-to-cost ratio compared to open-source codes such as ABINIT where QE will usually excel in scalability and integration into toolchains and to commercial competitors such as VASP, which are more user-friendly but with costly licensing fees. Its flexibility, healthy ecosystem, and open science commitment make it a best choice for high-precision simulations for computational materials science.

4

Results

4.1 Introduction

In recent years, the quest for efficient thermoelectric materials has intensified, driven by the urgent need to develop sustainable technologies capable of converting waste heat into usable electrical energy. Thermoelectric devices, which enable direct energy conversion between heat and electricity, are characterized by their efficiency parameter, the dimensionless figure of merit (ZT). High ZT values require a rare combination of high electrical conductivity, high Seebeck coefficient, and low thermal conductivity — a challenging balance to achieve in a single material. Among the promising candidates, Double half-Heusler compounds have emerged as particularly attractive owing to their tunable structural, electronic, and thermal properties.

Double half-Heuslers, with a general formula of $X_2YY'Z_2$, extend the classic half-Heusler structure by incorporating two formula units and offering greater flexibility in elemental substitution and electronic structure engineering. This structural complexity often leads to enhanced phonon scattering, naturally reducing lattice thermal conductivity without significantly deteriorating the electronic transport properties — a crucial requirement for high-performance thermoelectric materials. Moreover, their mechanical stability, wide range of possible band gaps, and strong thermal robustness further make double half-Heuslers excellent candidates for thermoelectric applications operating across diverse temperature ranges.

In this thesis, a detailed theoretical investigation is conducted on three double half-Heusler compounds: $Ti_2Os\mathbf{Ni}Sb_2$, $Ti_2Os\mathbf{Pt}Sb_2$ and $Ti_2Os\mathbf{Pd}Sb_2$. These materials are selected based on the expectation that the heavy elements (**Os**, **Pt**, **Pd**) will contribute to low lattice thermal conductivity, while the titanium-based framework may ensure structural integrity and favorable electronic characteristics. Through first-principles calculations and Boltzmann transport theory, we will systematically explore their structural, mechanical, electronic, thermodynamic, and thermoelectric properties. Particular emphasis is placed on understanding their stability, electrical transport performance, and intrinsic thermal conductivity, with the aim of evaluating their potential in next-generation thermoelectric devices.

By shedding light on the fundamental properties of these Ti-based double half-Heuslers, this study aims to contribute valuable insights into the design and optimization of new materials for efficient thermoelectric energy conversion.

4.2 Computational Details

We have performed a numerical study using first-principles DFT to calculate the electronic crystal structure of the double half-Heusler compounds $Ti_2Os\mathbf{Ni}Sb_2$, $Ti_2Os\mathbf{Pt}Sb_2$ and $Ti_2Os\mathbf{Pd}Sb_2$ (Fig. 4.4). DFT calculations were performed using the Quantum ESPRESSO package. Quantum ESPRESSO is based on DFT, plane wave (PW) basis sets, and pseudopotentials (both normconserving and ultrasoft). A kinetic energy PW cutoff of 90Ry was used. The electronic density of states (DOS) was calculated using a *k-mesh* of $9 \times 9 \times 9$ for nonselfconsistent-field calculations and the tetrahedron method, which is preferred over smearing methods for semiconductors. We used PBE-GGA exchangecorrelation (XC) functional for structure optimization and EVGGA (it provides more precise results for the band gap of semiconductors) for calculating the electronic structure (PDOS and band structure) with ultrasoft pseudopotentials distributed by the pslibrary 1.0.0 (`https://dalcorso.github.io/pslibrary/`), a library of ultrasoft and PAW pseudopotentials. PBEsol-GGA XC functional was used to compute the ECs at 0K, using the stress–strain relationship as implemented in the Thermo_pw code using the Marzari–Vanderbilt smearing approach and a smearing parameter of 0.05.

κ_L calculations:

The lattice thermal conductivity κ_L was estimated using the Slack model, which provides a reliable approach based on elastic constants. This method offers a favorable balance between computational efficiency and accuracy, avoiding the high computational cost associated with full phonon dispersion or anharmonic phonon calculations. Despite its simplicity, the Slack model yields results that are generally consistent with more intensive methods.

4.3 Convergence testing

The initial values for the plane-wave cutoff energy (ecutwfc) and the charge density cutoff energy (ecutrho) can be obtained from the pseudopotential files used in the calculations. As a starting point, the highest recommended values of *ecutwfc* and *ecutrho* among the selected pseudopotentials are chosen. These initial values are then systematically tested through convergence testing to determine the optimal cutoffs that provide a good balance between computational efficiency and the accuracy of the results.

```
Suggested minimum cutoff for wavefunctions:  75. Ry
Suggested minimum cutoff for charge density: 476. Ry
```

The hydrostatic pressure P on a given unit cell is an experimentally observable property that is rather sensitive to numerical precision. If this property is converged with respect to *k-mesh*, many other less sensitive properties will be converged too. Therefore, it is a good idea to monitor the hydrostatic pressure.

The calculation time increases with increasing *k-mesh*. That's why we cannot simply take by default a very dense and safe k-mesh: the calculations would take way too long. If our k-mesh is too coarse ($3 \times 3 \times 3$) then our calculation is superfast (362.96 seconds only), but the predicted hydrostatic pressure is meaningless. A compromise must be reached.

If we try a denser *k-mesh*: the predicted pressure changes from 25 to $\approx$ 2kbar. If we keep increasing the k-mesh density, the hydrostatic pressure stabilizes around 1.6kbar. It is a good compromise to set the k-mesh to $9 \times 9 \times 9$.

The calculation time increases with the value of $ecutwfc$, hence also for this parameter it is important to select the minimal value that gives us the converged result.

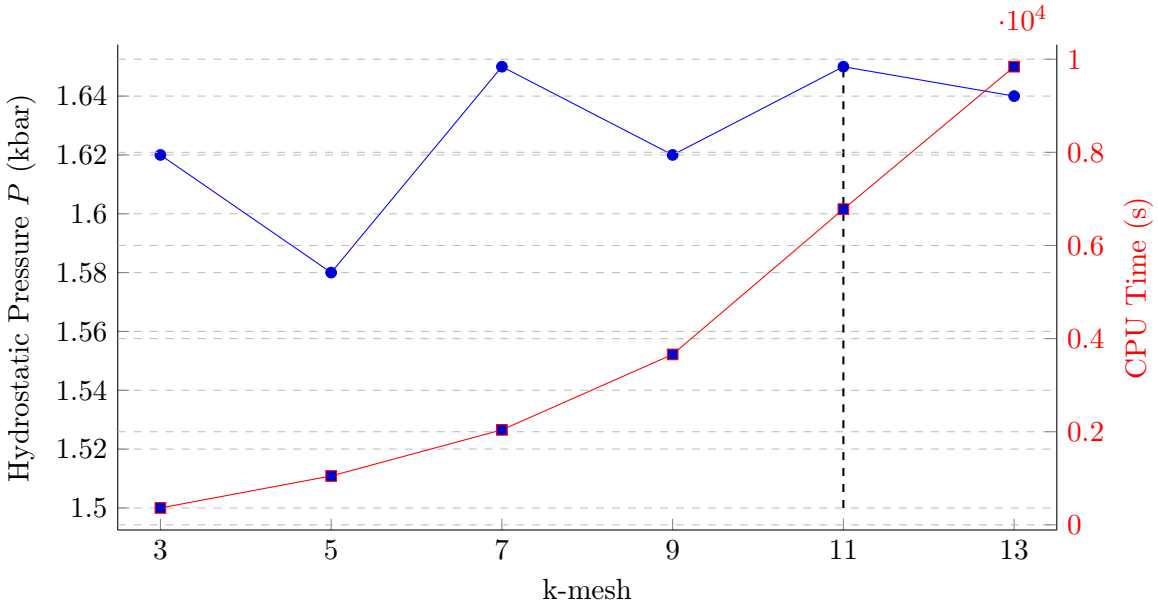

Figure 4.1: Hydrostatic pressure and CPU time vs. *k-mesh*. CPU time converted to seconds.

k-mesh	E_{tot}	P	CPU time
$1 \times 1 \times 1$	-1636.77564471	25.57	1m 40.81s
$3 \times 3 \times 3$	-1636.97904120	1.62	6m 2.96s
$5 \times 5 \times 5$	-1636.97923234	1.58	17m 29.57s
$7 \times 7 \times 7$	-1636.97922577	1.65	33m59.98s
$9 \times 9 \times 9$	-1636.97923239	1.62	1h 1m
$11 \times 11 \times 11$	-1636.97924181	1.65	1h53m
$13 \times 13 \times 13$	-1636.97923510	1.64	2h44m

Table 4.1: Evolution of hydrostatic pressure P ($kbar$), total energy E_{tot} (Ry), and CPU time (s) with respect to the number of sampling points (*k-mesh*).

ecutwfc (Ry)	E_{tot}	P	CPU time
25	-1610.47147606	-8633.35	20m10.09s
35	-1633.66513849	-1588.46	15m13.00s
45	-1636.62506545	-236.15	26m58.05s
55	-1636.94440311	-12.48	36m27.83s
65	-1636.96567594	5.27	49m 1.43s
75	-1636.97923239	1.62	1h 1m
85	-1636.99283077	3.78	1h20m
95	-1636.99921316	7.30	1h37m
105	-1637.00097992	8.63	2h13m
115	-1637.00170571	8.68	2h14m

Table 4.2: Evolution of hydrostatic pressure P ($kbar$), total energy E_{tot} (Ry), and CPU time (s) with respect to the plane-wave basis set size for the wavefunctions (*ecutwfc*).

N	*ecutrho* (Ry)	E_{tot}	P	CPU time
2	190	-1637.00731516	10.31	1h17m
3	285	-1637.00018799	7.38	1h16m
4	380	-1636.99941050	7.35	1h29m
5	475	-1636.99936407	7.35	1h28m
6	570	-1636.99924904	7.32	1h31m
7	665	-1636.99926742	7.33	1h35m
8	760	-1636.99921316	7.30	1h39m

Table 4.3: Evolution of hydrostatic pressure P ($kbar$), total energy E_{tot} (Ry), and CPU time (s) with respect to the basis set size ($ecutrho = ecutwfc \times N$).

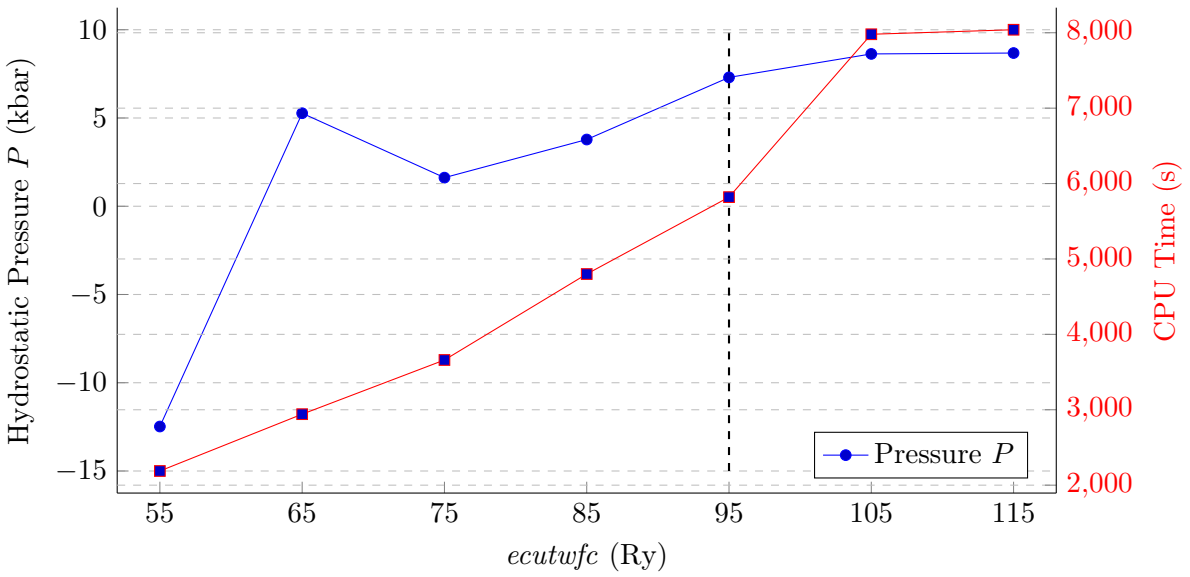

Figure 4.2: Hydrostatic pressure and CPU time vs. cutoff energy (*ecutwfc*).

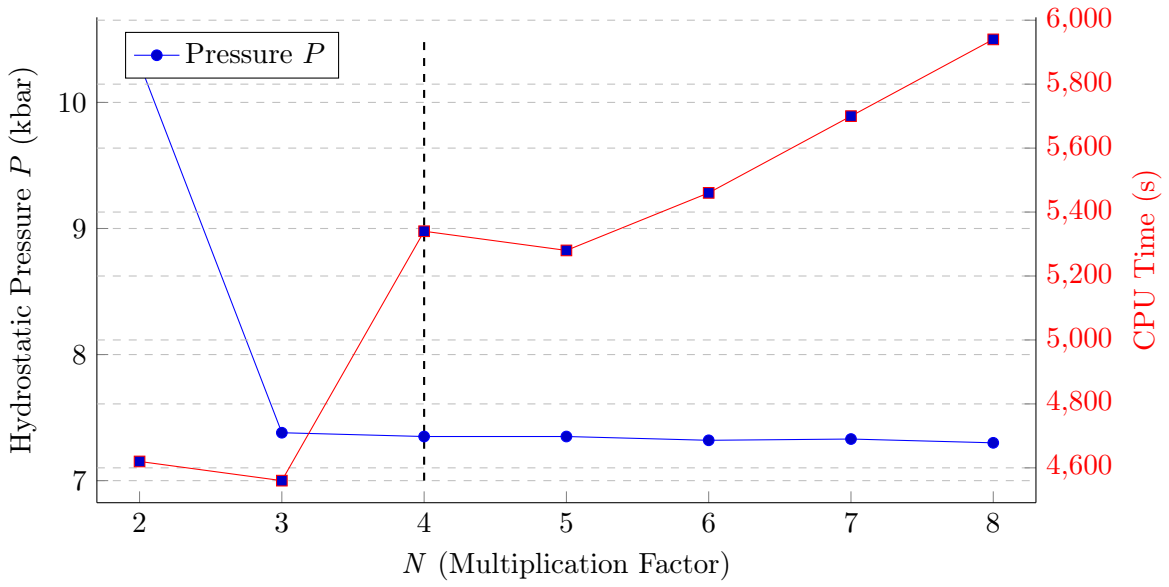

Figure 4.3: Hydrostatic pressure and CPU time vs. basis set multiplication factor N.

Compound	$a = b$	c/a	V_0	ΔE_f	B	B'
$Ti_2OsNiSb_2$	6.086	2.00	450.84	-0.478	143.89	4.32
	6.076 [82]	1.99	446.23	−0.538	-0.731	–
$Ti_2OsPtSb_2$	6.207	2.00	478.74	-0.731	150.73	4.81
	6.189 [82]	2.00	473.28	−0.664	–	–
$Ti_2OsPdSb_2$	6.194	2.00	475.27	-0.637	141.91	4.91
	6.191 [82]	1.99	472.67	−0.571	–	–

Table 4.4: The table lists the structural parameters of tetragonal $Ti_2Os\mathbf{Y}'Sb_2$ double half-Heusler compounds, including lattice constant a (in Å), c/a ratio, ground state volume V_0 (in Å^3), bulk modulus B (in GPa), and its pressure derivative B' (dimensionless).

4.4 Ground-state structure

An illustration of the structural arrangement of these compounds is presented in Figure 4.4. Table 4.5 presents the structural parameters of these compounds, which were obtained from the energy–volume (E–V) curves, offering insights into their optimized lattice configurations.

$$E(V) = E_0 + \frac{9V_0B_0}{16}\left\{\left[\left(\frac{V_0}{V}\right)^{2/3} - 1\right]^3 B_0' + \left[\left(\frac{V_0}{V}\right)^{2/3} - 1\right]^2 \left[6 - 4\left(\frac{V_0}{V}\right)^{2/3}\right]\right\} \tag{4.2}$$

The OQMD [82, 83] values served as a starting point for further structural optimization of the lattice parameter a and the c/a ratio. As expected, all three compounds exhibit *non-magnetic* behavior, consistent with the observation that magnetic properties in Heusler alloys typically arise only when elements such as Co or Mn are present.

The calculated lattice constants a (6.086Å, 6.207Å, and 6.194Å for the Ni, Pt, and Pd-based compounds, respectively.) and corresponding c/a ratios are in good agreement with the values reported in the OQMD database [82], differing by less than 0.3%, which validates the accuracy of the structural optimization method employed in this work. All three compounds exhibit a tetragonal symmetry with $c/a = 2.00$, indicating a consistent crystal structure across the Y' substitutions. The equilibrium volume V_0 increases with the atomic radius of the Y' element (Ni < Pd < Pt), from 450.84Å^3 for $Ti_2OsNiSb_2$ to 478.74Å^3 for $Ti_2OsPtSb_2$. This trend is consistent with the increase in atomic size from Ni to Pt, which leads to an overall expansion of the unit cell.

The bulk modulus B is: 143.89GPa for $Ti_2OsNiSb_2$, 141.91GPa for $Ti_2OsPdSb_2$, and 150.73GPa for $Ti_2OsPtSb_2$. While $Ti_2OsPdSb_2$ is slightly softer, $Ti_2OsPtSb_2$ is the stiffest among the three, suggesting that the Pt-containing compound is more resistant to volume compression.

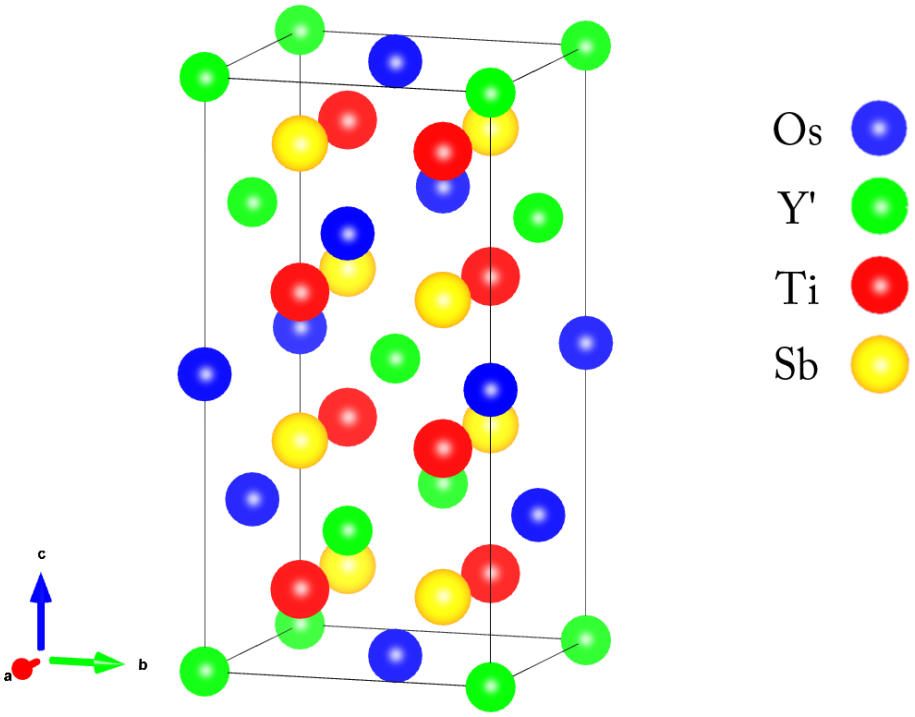

Figure 4.4: Crystal structure of $Ti_2OsY'Sb_2$ (Y': Ni, Pt, Pd) Double half-Heusler compounds. The *blue*, *green*, *red* and *yellow* spheres represent the Os, Y', Ti and Sb atoms, respectively.

Compound	*Atom*	*Wyck. pos.*	x	y	z
$Ti_2OsY'Sb_2$	Ti	$8d$	-0.250	0.250	0.125
	Os	$4a$	0.000	0.000	0.500
	Y'	$4b$	0.000	0.000	0.000
	Sb	$8d$	0.250	0.250	0.125

Table 4.5: *Wyckoff positions* and *atomic coordinates* for $Ti_2OsY'Sb_2$.

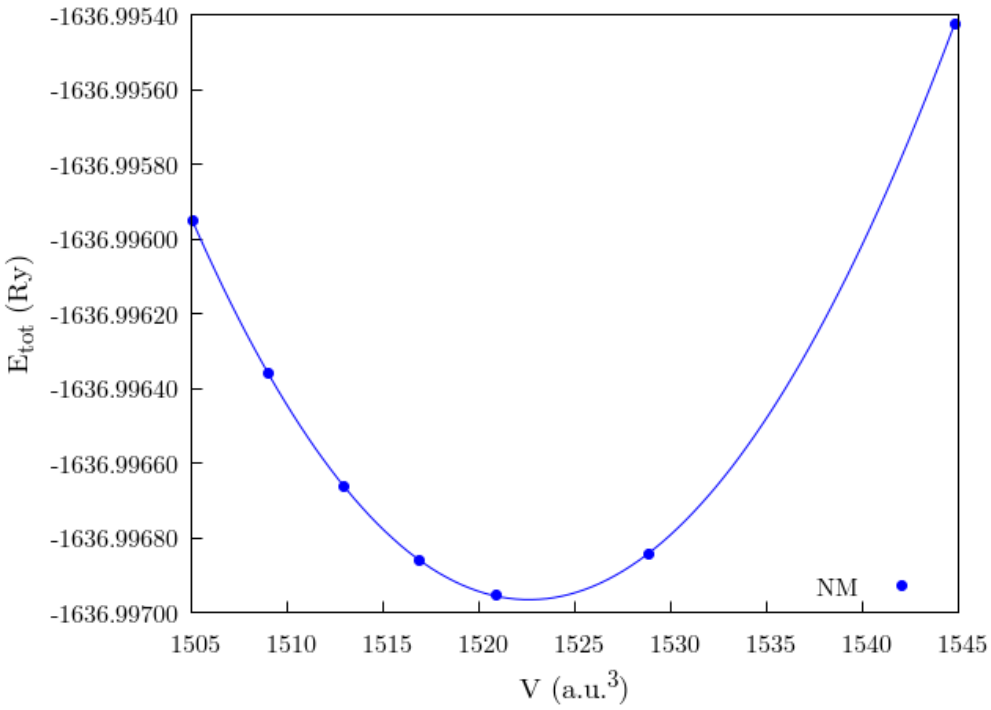

Figure 4.5: Energy–volume curve for $Ti_2OsNiSb_2$ fitted using the third-order Birch–Murnaghan equation of state. The discrete *blue* points represent the DFT-calculated total energies, while the solid line corresponds to the fitted equation, indicating the *equilibrium volume* V_0 and *minimum energy configuration* E_0.

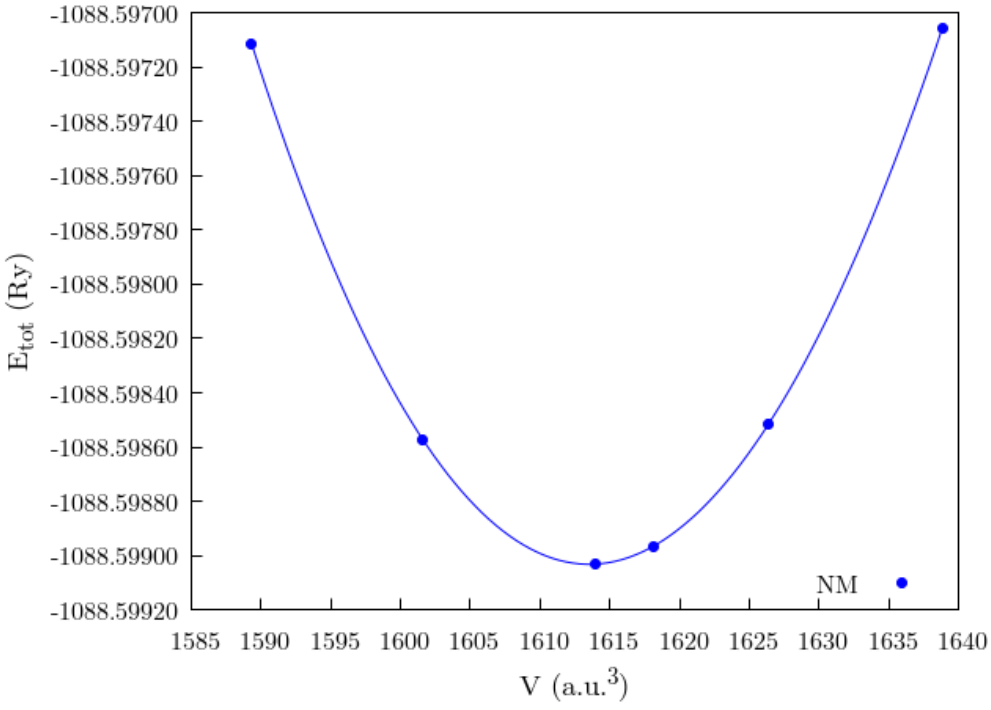

Figure 4.6: Energy–volume curve for $Ti_2OsPtSb_2$.

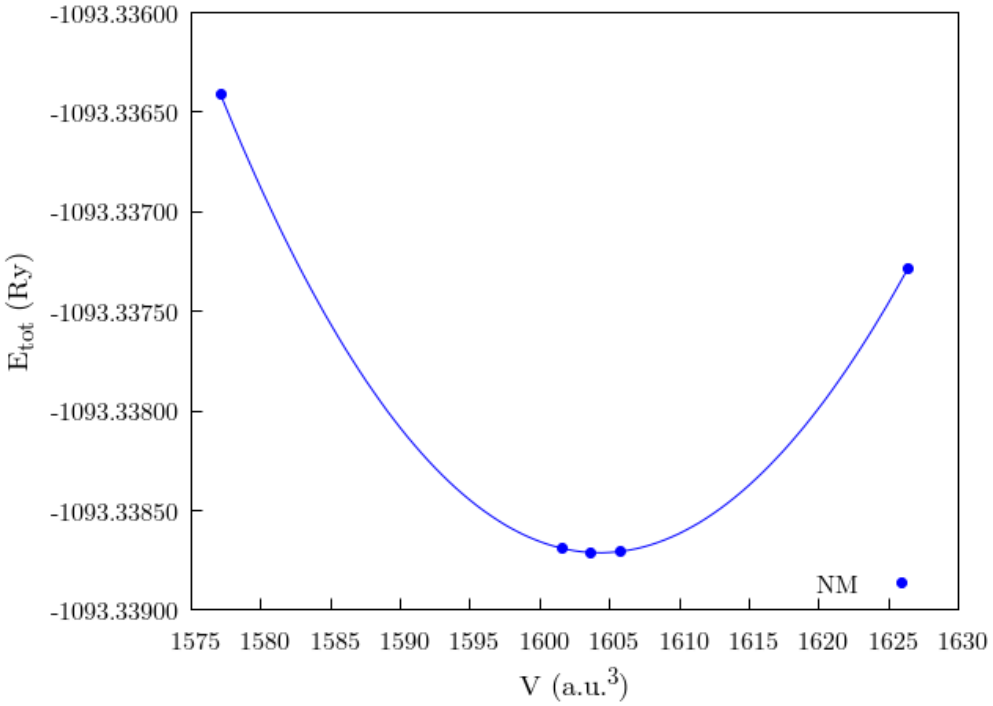

Figure 4.7: Energy–volume curve for $Ti_2OsPdSb_2$.

4.5 Electronic properties

Double Heusler compounds with a valence electron count (VEC) of 18 typically exhibit semiconducting behavior. This is due to the fact that a VEC of 18 leads to a completely filled valence band and an empty conduction band, resulting in a band gap at the Fermi level. Consequently, all double Heusler compounds with a total of 18 valence electrons per formula unit are expected to be semiconductors.

The obtained band structures of the $Ti_2OsNiSb_2$, $Ti_2OsPtSb_2$, and $Ti_2OsPdSb_2$ double half-Heusler compounds, shown in Figures 4.11, 4.12 and 4.13, reveals a semiconducting nature with a narrow indirect band gap (Table 4.6). The electronic bands are plotted along high-symmetry directions in the Brillouin zone, including Γ, X, Y, Σ, Σ_1, N, P, Y_1, and Z. The valence band maximum (VBM) and conduction band minimum (CBM) occur at different k-points, indicating an indirect band gap. This is typical for many Heusler compounds. The Fermi level E_f is marked with a blue dashed line, intersecting a region between the valence and conduction bands, confirming the material is semiconducting.

Near the Fermi level, the bands exhibit moderate curvature, suggesting relatively low effective masses for charge carriers — a desirable feature for high mobility applications in thermoelectrics.

The projected density of states (PDOS) provides critical insights into the orbital and atomic contributions to the electronic states near the Fermi level, aiding the understanding of bonding and conduction mechanisms. The Total DOS plot shows a clear pseudo-gap at the Fermi level, confirming

the semiconducting character of the compound. A sharp increase in states just above and below the Fermi level suggests a narrow band gap, consistent with the band structure results. The total DOS also exhibits multiple peaks in the valence region, indicating hybridized states from different atoms.

In $Ti_2OsNiSb_2$ (Fig. 4.8), the valence band is primarily composed of Ni(d) and Sb(p) states, while the conduction band edge is dominated by Ti(d) states. This indicates strong d–p hybridization, typical of Heusler compounds, with Ni playing a central role in valence band formation.

For $Ti_2OsPtSb_2$ (Fig. 4.9), the band gap appears slightly wider. The Pt(d) states are more delocalized than Ni(d), contributing broadly to both the mid-valence and deep valence bands. The Ti(d) states still dominate near the conduction band edge.

In $Ti_2OsPdSb_2$ (Fig. 4.10), the PDOS is also consistent with semiconducting behavior, but the band gap appears slightly narrower than in the Pt-based analog. Pd(d) states dominate the mid-to-lower valence band, while the conduction band is again governed by Ti(d) contributions. Sb(p) states are prominent throughout the valence band, particularly below 2eV, across all three compounds.

Compound	E_g (eV)
$Ti_2OsNiSb_2$	≈ 0.4
	0.381 [82]
$Ti_2OsPtSb_2$	≈ 0.9
	1.140 [82]
$Ti_2OsPdSb_2$	≈ 0.7
	0.930 [82]

Table 4.6: Table comparing the computed band gap energies (E_g) with those reported in the Open Quantum Materials Database (OQMD), highlighting agreement and deviations for selected compounds.

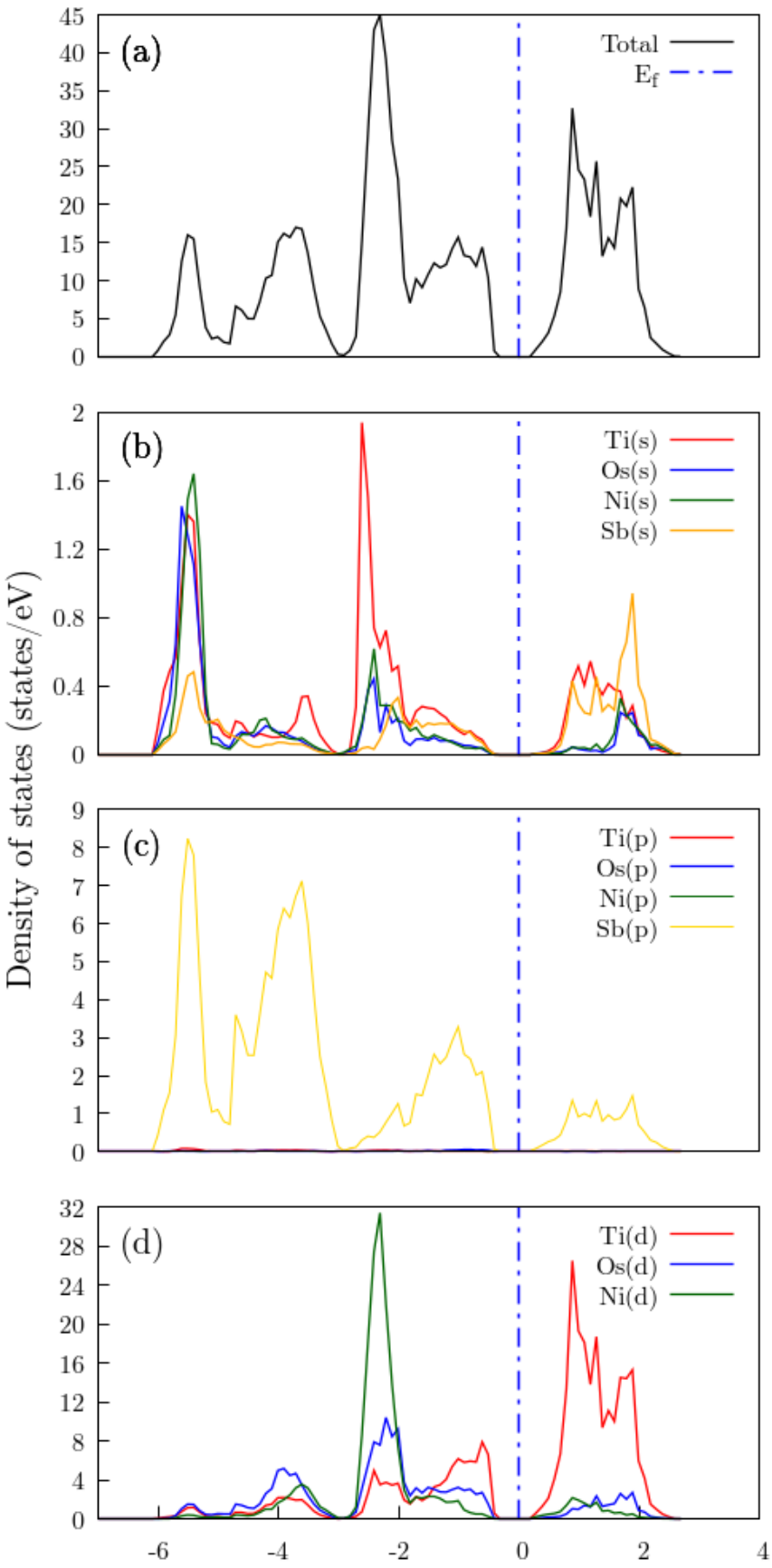

Figure 4.8: Partial density of states (PDOS) of $Ti_2Os\mathbf{Ni}Sb_2$ double Heusler compound showing the contribution of Ti, Os, Ni, and Sb atomic orbitals to the electronic states near the Fermi level (E_f).

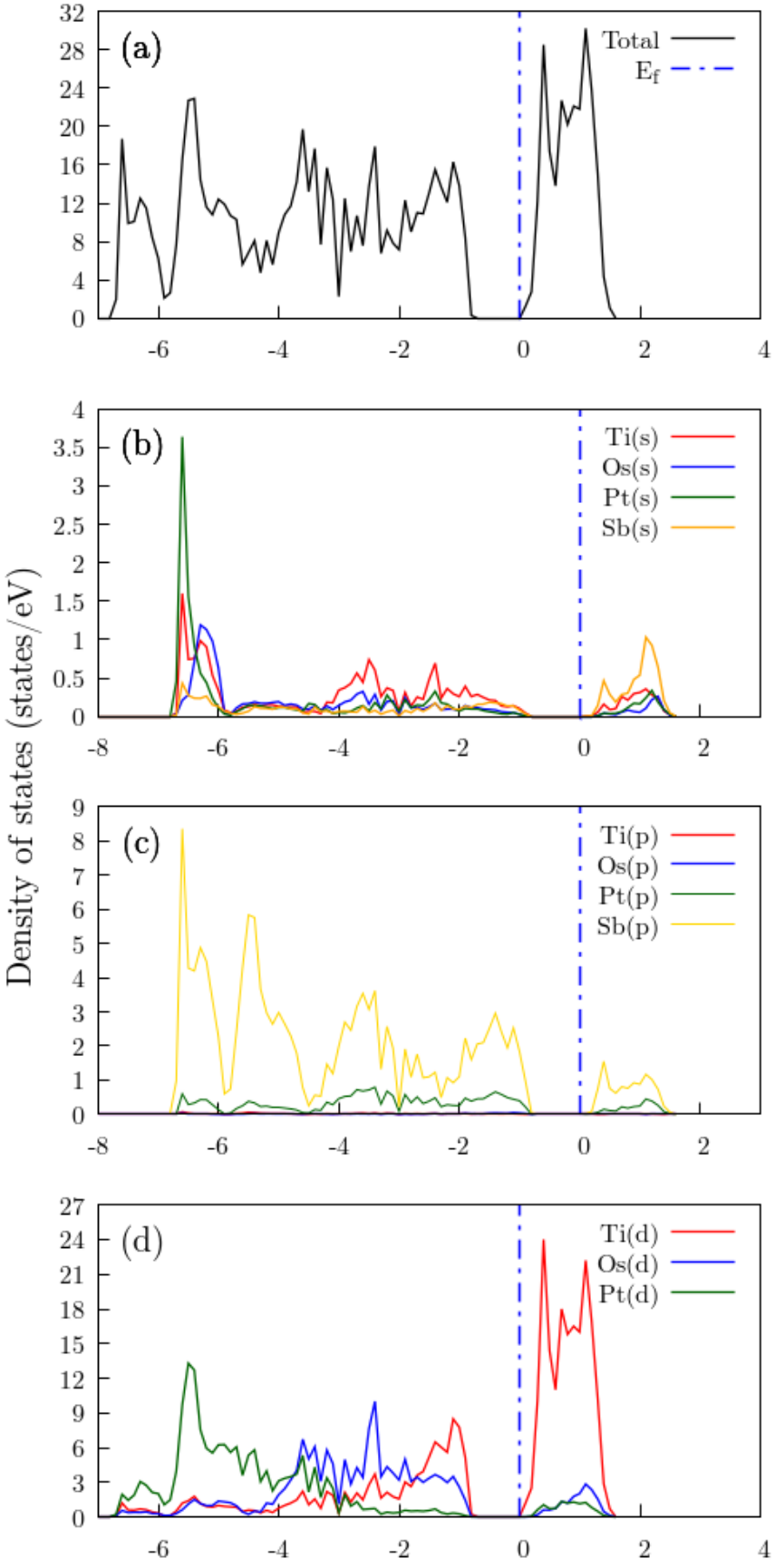

Figure 4.9: Partial density of states (PDOS) of $Ti_2Os\mathbf{Pt}Sb_2$.

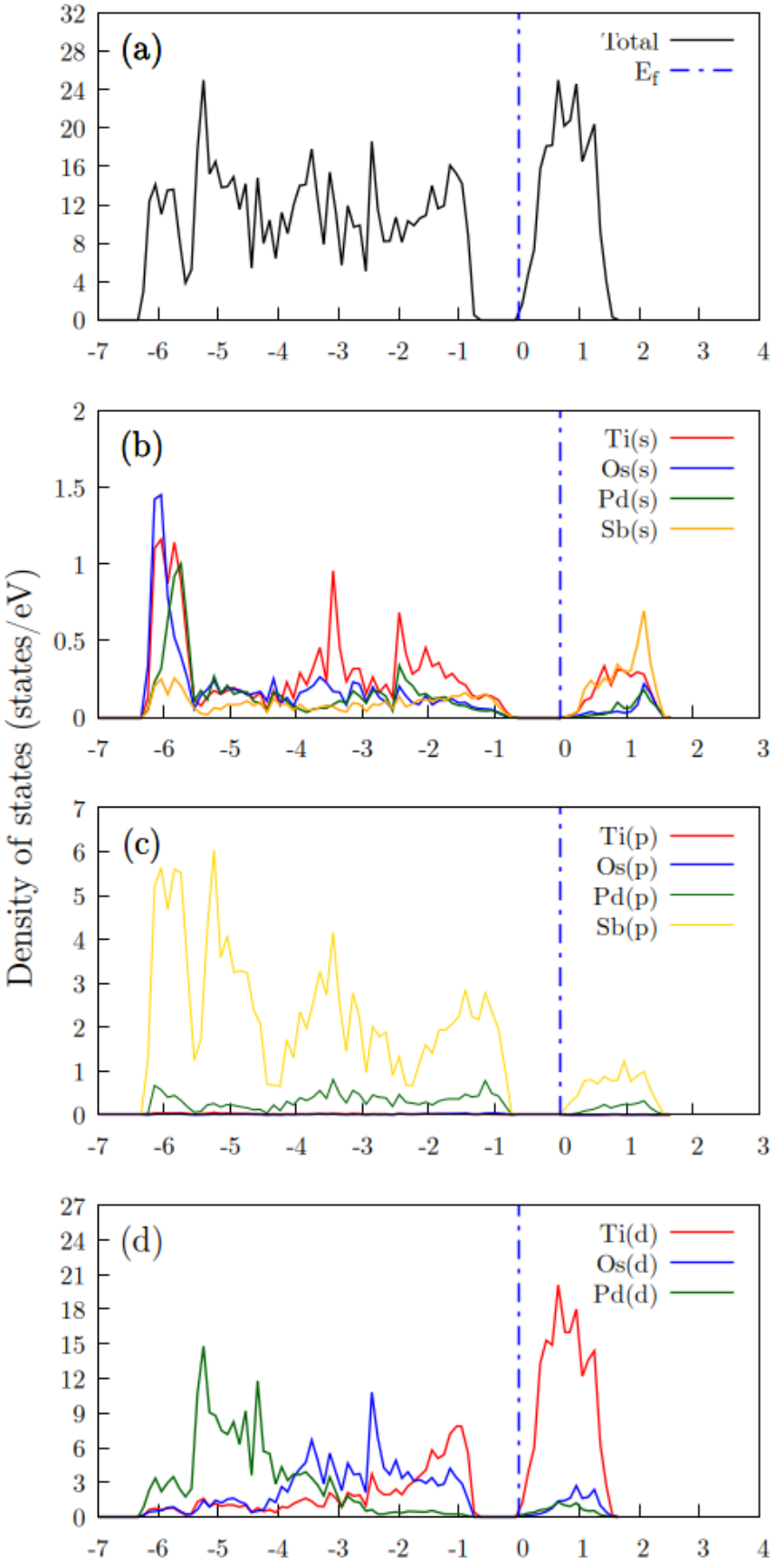

Figure 4.10: Partial density of states (PDOS) of $Ti_2Os\mathbf{Pd}Sb_2$.

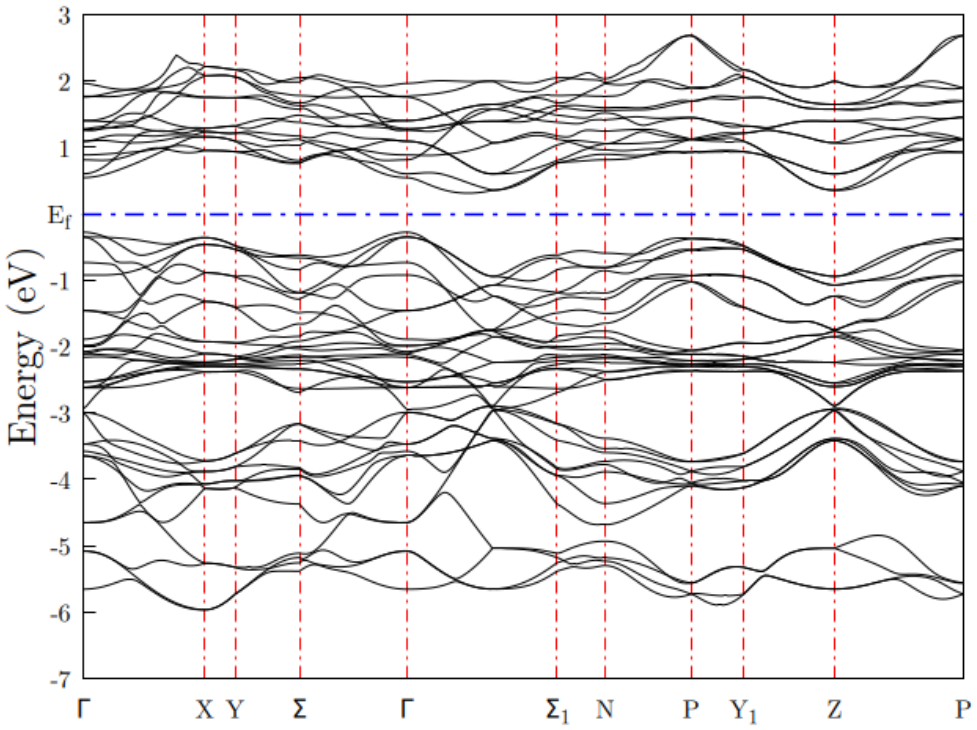

Figure 4.11: Electronic band structure of $Ti_2Os\mathbf{Ni}Sb_2$ calculated using DFT with the PBE functional. The Fermi level is set to zero. The compound exhibits semiconducting behavior with an indirect band gap.

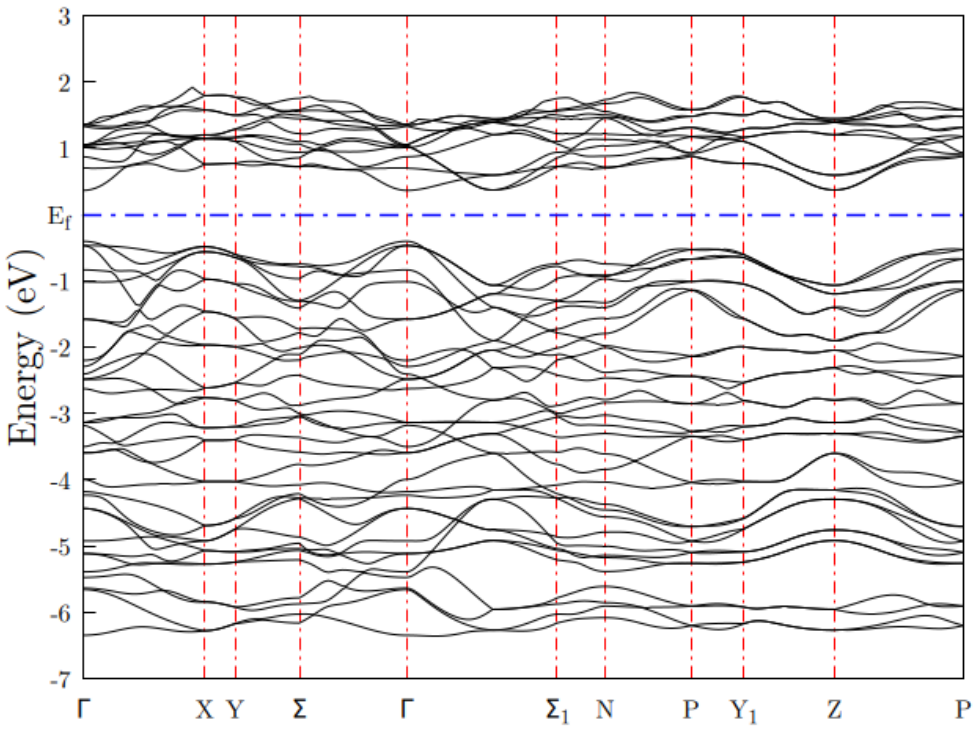

Figure 4.12: Electronic band structure of $Ti_2Os\mathbf{Pt}Sb_2$. The compound exhibits semiconducting behavior with an indirect band gap.

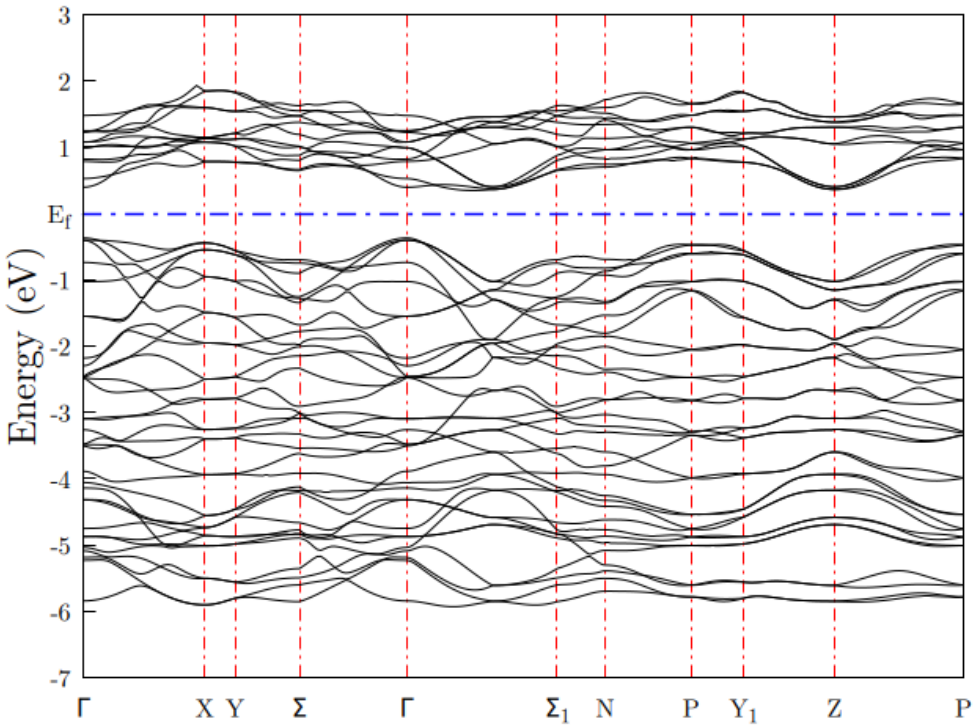

Figure 4.13: Electronic band structure of $Ti_2Os\mathbf{Pd}Sb_2$. The compound exhibits semiconducting behavior with an indirect band gap.

5

Conclusion

In this dissertation, we have explored the potential of three Double half-Heusler compounds ($Ti_2Os\mathbf{Ni}Sb_2$, $Ti_2Os\mathbf{Pt}Sb_2$, $Ti_2Os\mathbf{Pd}Sb_2$) as promising candidates for thermoelectric applications. Through a comprehensive analysis of their structural, electronic and thermal properties, it is evident that they make them excellent thermoelectric materials.

One of the primary advantages of Double half-Heusler compounds lies in their *flexible crystal structure*, which allows for extensive chemical tunability and site substitution. This flexibility enables the optimization of electronic band structures to achieve high Seebeck coefficients and desirable electrical conductivities. Additionally, many Double half-Heusler compounds exhibit *intrinsic low lattice thermal conductivity* κ_L due to their *complex unit cells*, which is a key requirement for enhancing the thermoelectric figure of merit (ZT).

Overall, double half-Heusler materials represent a new frontier in thermoelectric research, offering a versatile platform for the design of high-performance thermoelectric devices. Continued theoretical and experimental efforts are expected to unlock even greater efficiencies and pave the way for their integration into waste heat recovery systems, solid-state cooling technologies, and sustainable energy solutions.

Bibliography

[1] Fr Heusler and Fritz Richarz. Studien über magnetisierbare manganlegierungen. *Zeitschrift für anorganische Chemie*, 61(1):265–279, 1909.

[2] Albert James Bradley and JW Rodgers. The crystal structure of the heusler alloys. *Proceedings of the royal society of london. Series A, Containing Papers of a Mathematical and Physical Character*, 144(852):340–359, 1934.

[3] DP Rai, A Shankar, Sandeep, MP Ghimire, and RK Thapa. Electronic and magnetic properties of a full-heusler alloy co 2 crge: a first-principles study. *Journal of Theoretical and Applied Physics*, 7:1–6, 2013.

[4] Khadejah M Al-Masri, Mohammed S Abu-Jafar, Mahmoud Farout, Diana Dahliah, Ahmad A Mousa, Said M Azar, and Rabah Khenata. Structural, elastic, electronic, and magnetic properties of full-heusler alloys sc2tial and sc2tisi using the fp-lapw method. *Magnetochemistry*, 9(4):108, 2023.

[5] Jörg von Appen Dipl.-Chem. Heiko Lueken Prof. Dr. Rainer Niewa Dr. Richard Dronskowski Prof. Dr Andreas Houben Dipl.-Chem., Paul Müller Dr. Synthese, kristallstruktur und magnetische eigenschaften des halbharten itineranten ferromagneten rhfe3n. *angewandte chemie*, 117(44):7382, 2005.

[6] Elizabeth Decolvenaere, Michael Gordon, Ram Seshadri, and Anton Van der Ven. First-principles investigation of competing magnetic interactions in (mn, fe) ru 2 sn heusler solid solutions. *Physical Review B*, 96(16):165109, 2017.

[7] LL Wang, L Miao, ZY Wang, W Wei, R Xiong, HJ Liu, J Shi, and XF Tang. Thermoelectric performance of half-heusler compounds tinisn and ticosb. *Journal of Applied Physics*, 105(1), 2009.

[8] G Joseph Poon. Electronic and thermoelectric properties of half-heusler alloys. In *Semiconductors and semimetals*, volume 70, pages 37–75. Elsevier, 2001.

[9] R A De Groot, F M Mueller, PG v van Engen, and KHJ Buschow. New class of materials: half-metallic ferromagnets. *Physical review letters*, 50(25):2024, 1983.

[10] K Mastronardi, D Young, C-C Wang, P Khalifah, RJ Cava, and AP Ramirez. Antimonides with the half-heusler structure: New thermoelectric materials. *Applied physics letters*, 74(10):1415–1417, 1999.

[11] Tanja Graf, Claudia Felser, and Stuart SP Parkin. Simple rules for the understanding of heusler compounds. *Progress in solid state chemistry*, 39(1):1–50, 2011.

[12] H Hohl, AP Ramirez, W Kaefer, K Fess, Ch Thurner, Ch Kloc, and E Bucher. A new class of materials with promising thermoelectric properties: Mnisn (m= ti, zr, hf). *MRS Online Proceedings Library (OPL)*, 478:109, 1997.

[13] FG Aliev, NB Brandt, VV Moshchalkov, VV Kozyrkov, RV Skolozdra, and AI Belogorokhov. Gap at the fermi level in the intermetallic vacancy system rbisn (r= ti, zr, hf). *Zeitschrift für Physik B Condensed Matter*, 75:167–171, 1989.

[14] S Bhattacharya, AL Pope, RT Littleton IV, Terry M Tritt, V Ponnambalam, Y Xia, and SJ Poon. Effect of sb doping on the thermoelectric properties of ti-based half-heusler compounds, tinisn 1- x sb x. *Applied Physics Letters*, 77(16):2476–2478, 2000.

[15] Benjamin Balke, Gerhard H Fecher, Andrei Gloskovskii, Joachim Barth, Kristian Kroth, Claudia Felser, Rosa Robert, and Anke Weidenkaff. Doped semiconductors as half-metallic materials: Experiments and first-principles calculations of co ti 1- x m x sb (m= sc, v, cr, mn, fe). *Physical Review B—Condensed Matter and Materials Physics*, 77(4):045209, 2008.

[16] Chin Shan Lue, CF Chen, JY Lin, YT Yu, and YK Kuo. Thermoelectric properties of quaternary heusler alloys fe 2 val 1- x si x. *Physical Review B—Condensed Matter and Materials Physics*, 75(6):064204, 2007.

[17] Yoshisato Kimura, Hazuki Ueno, and Yoshinao Mishima. Thermoelectric properties of directionally solidified half-heusler (m 0.5 a, m 0.5 b) nisn (m a, m b= hf, zr, ti) alloys. *Journal of electronic materials*, 38:934–939, 2009.

[18] Jing-Feng Li, Wei-Shu Liu, Li-Dong Zhao, and Min Zhou. High-performance nanostructured thermoelectric materials. *NPG Asia Materials*, 2(4):152–158, 2010.

[19] Wenjie Xie, Anke Weidenkaff, Xinfeng Tang, Qingjie Zhang, Joseph Poon, and Terry M Tritt. Recent advances in nanostructured thermoelectric half-heusler compounds. *Nanomaterials*, 2(4):379–412, 2012.

[20] Stanislav Chadov, Xiaoliang Qi, Jürgen Kübler, Gerhard H Fecher, Claudia Felser, and Shou Cheng Zhang. Tunable multifunctional topological insulators in ternary heusler compounds. *Nature materials*, 9(7):541–545, 2010.

[21] Qiang Gao, Ingo Opahle, and Hongbin Zhang. High-throughput screening for spin-gapless semiconductors in quaternary heusler compounds. *Physical Review Materials*, 3(2):024410, 2019.

[22] Nuno M Fortunato, Xiaoqing Li, Stephan Schonecker, Ruiwen Xie, Andreas Taubel, Franziska Scheibel, Ingo Opahle, Oliver Gutfleisch, and Hongbin Zhang. High-throughput screening

of all-d-metal heusler alloys for magnetocaloric applications. *Chemistry of Materials*, 36(14):6765–6776, 2024.

[23] Jesús Carrete, Wu Li, Natalio Mingo, Shidong Wang, and Stefano Curtarolo. Finding unprecedentedly low-thermal-conductivity half-heusler semiconductors via high-throughput materials modeling. *Physical Review X*, 4(1):011019, 2014.

[24] Leonie Gomell, Imants Dirba, Hanna Bishara, Zhongji Sun, Łukasz Żrodowski, Tomasz Choma, Bartosz Morończyk, Gerhard Dehm, Konstantin P Skokov, Oliver Gutfleisch, et al. Microstructure of a spark-plasma-sintered fe2val-type heusler alloy for thermoelectric application. *arXiv preprint arXiv:2307.05051*, 2023.

[25] Degang Zhao, Lin Wang, Lin Bo, and Di Wu. Synthesis and thermoelectric properties of ni-doped zrcosb half-heusler compounds. *Metals*, 8(1):61, 2018.

[26] Lukas Wollmann, Ajaya K Nayak, Stuart SP Parkin, and Claudia Felser. Heusler 4.0: tunable materials. *Annual Review of Materials Research*, 47(1):247–270, 2017.

[27] Kelvin Elphick, William Frost, Marjan Samiepour, Takahide Kubota, Koki Takanashi, Hiroaki Sukegawa, Seiji Mitani, and Atsufumi Hirohata. Heusler alloys for spintronic devices: review on recent development and future perspectives. *Science and technology of advanced materials*, 22(1):235–271, 2021.

[28] F Casper, T Graf, S Chadov, B Balke, and C Felser. Half-heusler compounds: novel materials for energy and spintronic applications. *Semiconductor Science and Technology*, 27(6):063001, 2012.

[29] I Galanakis, Ph Mavropoulos, and Ph H Dederichs. Electronic structure and slater–pauling behaviour in half-metallic heusler alloys calculated from first principles. *Journal of Physics D: Applied Physics*, 39(5):765, 2006.

[30] Justin A Mayer and Ram Seshadri. Electron count dictates phase separation in heusler alloys. *Physical Review Materials*, 6(5):054406, 2022.

[31] MI Katsnelson, V Yu Irkhin, Liviu Chioncel, AI Lichtenstein, and Robert A de Groot. Half-metallic ferromagnets: From band structure to many-body effects. *Reviews of Modern Physics*, 80(2):315–378, 2008.

[32] Fabian Garmroudi, Michael Parzer, Takao Mori, Andrej Pustogow, and Ernst Bauer. Thermoelectric transport in ru 2 ti si full-heusler compounds. *PRX Energy*, 4(1):013010, 2025.

[33] Shashwat Anand, Ramya Gurunathan, Thomas Soldi, Leah Borgsmiller, Rachel Orenstein, and G Jeffrey Snyder. Thermoelectric transport of semiconductor full-heusler vfe 2 al. *Journal of Materials Chemistry C*, 8(30):10174–10184, 2020.

[34] Markus Meinert, Jan-Michael Schmalhorst, and Günter Reiss. Exchange interactions and curie temperatures ofmn2coz compounds. *Journal of Physics: Condensed Matter*, 23(11):116005, 2011.

[35] Kelvin Elphick, William Frost, Marjan Samiepour, Takahide Kubota, Koki Takanashi, Hiroaki Sukegawa, Seiji Mitani, and Atsufumi Hirohata. Heusler alloys for spintronic devices: review on recent development and future perspectives. *Science and technology of advanced materials*, 22(1):235–271, 2021.

[36] Riaz Ahamed Ahamed Khan, Reza Ghomashchi, Zonghan Xie, and Lei Chen. Ferromagnetic shape memory heusler materials: Synthesis, microstructure characterization and magnetostructural properties. *Materials*, 11(6):988, 2018.

[37] Wikipedia contributors. Heusler compound, 2025. Accessed on 30 May 2025.

[38] Shuo Chen and Zhifeng Ren. Recent progress of half-heusler for moderate temperature thermoelectric applications. *Materials today*, 16(10):387–395, 2013.

[39] Kaiyang Xia, Chaoliang Hu, Chenguang Fu, Xinbing Zhao, and Tiejun Zhu. Half-heusler thermoelectric materials. *Applied Physics Letters*, 118(14), 2021.

[40] Airan Li, Madison K Brod, Yuechu Wang, Kejun Hu, Pengfei Nan, Shen Han, Ziheng Gao, Xinbing Zhao, Binghui Ge, Chenguang Fu, et al. Opening the bandgap of metallic half-heuslers via the introduction of d–d orbital interactions. *Advanced Science*, 10(23):2302086, 2023.

[41] Maxwell T Dylla, Alexander Dunn, Shashwat Anand, Anubhav Jain, and G Jeffrey Snyder. Machine learning chemical guidelines for engineering electronic structures in half-heusler thermoelectric materials. *Research*, 2020.

[42] Justin A Mayer and Ram Seshadri. Electron count dictates phase separation in heusler alloys. *Physical Review Materials*, 6(5):054406, 2022.

[43] Slimane Gheriballah, A Chahed, Y Benazzouzi, and H Rozale. Structural, mechanical, electronic, and thermoelectric properties of new semiconducting d0 quaternary heusler compounds caknaz (z= si, ge, sn). a density functional theory study. *Revista mexicana de física*, 68(5), 2022.

[44] Bharti Gurunani and Dinesh C Gupta. Probing the thermoelectric and optical performance of half-heusler ptzrx (x= si, ge) semiconductors: a first principles investigation. *Materials Advances*, 5(23):9340–9358, 2024.

[45] Federico Serrano-Sánchez, Ting Luo, Junjie Yu, Wenjie Xie, Congcong Le, Gudrun Auffermann, Anke Weidenkaff, Tiejun Zhu, Xinbing Zhao, José A Alonso, et al. Thermoelectric properties of n-type half-heusler nbcosn with heavy-element pt substitution. *Journal of Materials Chemistry A*, 8(29):14822–14828, 2020.

[46] Patrick Hermet, Kinga Niedziolka, and Philippe Jund. A first-principles investigation of the thermodynamic and mechanical properties of ni–ti–sn heusler and half-heusler materials. *RSC Advances*, 3(44):22176–22184, 2013.

[47] Claudia Felser, Lukas Wollmann, Stanislav Chadov, Gerhard H Fecher, and Stuart SP Parkin. Basics and prospective of magnetic heusler compounds. *APL materials*, 3(4), 2015.

[48] Van An Dinh, Kazunori Sato, and Hiroshi Katayama-Yoshida. New high-t c half-heusler ferromagnets nimnz (z= si, p, ge, as). *Journal of the Physical Society of Japan*, 77(1):014705, 2008.

[49] Wenjie Xie, Anke Weidenkaff, Xinfeng Tang, Qingjie Zhang, Joseph Poon, and Terry M Tritt. Recent advances in nanostructured thermoelectric half-heusler compounds. *Nanomaterials*, 2(4):379–412, 2012.

[50] Sergey V Faleev, Yari Ferrante, Jaewoo Jeong, Mahesh G Samant, Barbara Jones, and Stuart SP Parkin. Heusler compounds with perpendicular magnetic anisotropy and large tunneling magnetoresistance. *Physical Review Materials*, 1(2):024402, 2017.

[51] Antti Karttunen. Heusler alloys. 2023.

[52] Asma Wederni, Jason Daza, Wael Ben Mbarek, Joan Saurina, Lluisa Escoda, and Joan-Josep Suñol. Crystal structure and properties of heusler alloys: a comprehensive review. *Metals*, 14(6):688, 2024.

[53] Susanta K Mohanta, Yongxue Tao, Xiaoyan Yan, Guanhua Qin, Venkatesh Chandragiri, Xi Li, Chao Jing, Shixun Cao, Jincang Zhang, Zhenhua Qiao, et al. First principles electronic structure and magnetic properties of inverse heusler alloys x2yz (x= cr; y= co, ni; z= al, ga, in, si, ge, sn, sb). *Journal of Magnetism and Magnetic Materials*, 430:65–69, 2017.

[54] Srikrishna Ghosh and Subhradip Ghosh. Systematic understanding of half-metallicity of ternary compounds in heusler and inverse heusler structures with 3d and 4d elements. *Physica Scripta*, 94(12):125001, 2019.

[55] S Skaftouros, Kemal Özdoğan, E Şaşıoğlu, and I Galanakis. Generalized slater-pauling rule for the inverse heusler compounds. *Physical Review B—Condensed Matter and Materials Physics*, 87(2):024420, 2013.

[56] DJ Mokhtari, Inshad Jum'h, H Baaziz, Z Charifi, T Ghellab, Ahmad Telfah, and Roland Hergenröder. Structural, electronic, magnetic and thermoelectric properties of inverse heusler alloys ti2cosi, mn2coal and cr2znsi by employing ab initio calculations. *Philosophical Magazine*, 100(12):1636–1661, 2020.

[57] Alexander P Kamantsev, Yuriy S Koshkid'ko, Ruslan Yu Gaifullin, Irek I Musabirov, Anatoliy V Koshelev, Alexey V Mashirov, Vladimir V Sokolovskiy, Vasiliy D Buchelnikov, Jacek Ćwik, and Vladimir G Shavrov. Inverse magnetocaloric effect in heusler ni44. 4mn36. 2sn14. 9cu4. 5 alloy at low temperatures. *Metals*, 13(12):1985, 2023.

[58] EC Passamani, F Xavier, E Favre-Nicolin, C Larica, AY Takeuchi, IL Castro, and JR Proveti. Magnetic properties of nimn-based heusler alloys influenced by fe atoms replacing mn. *Journal of applied physics*, 105(3), 2009.

[59] Md Rasheduzzaman, Khandaker Monower Hossain, SK Mitro, MA Hadi, Jibon Krishna Modak, and Md Zahid Hasan. Structural, mechanical, thermal, and optical properties of inverse-heusler alloys cr2coz (z= al, in): a first-principles investigation. *Physics Letters A*, 385:126967, 2021.

[60] David Michael Rowe. *Thermoelectrics handbook: macro to nano*. CRC press, 2005.

[61] Arman Molki. Simple demonstration of the seebeck effect. *Science Education Review*, 9(3):103–107, 2010.

[62] Corey Melnick and Massoud Kaviany. From thermoelectricity to phonoelectricity. *Applied Physics Reviews*, 6(2):021305, 2019.

[63] G. Jeffrey Snyder and Eric S. Toberer. Complex thermoelectric materials. *Nature Materials*, 7(2):105–114, 2008.

[64] Mercouri G. Kanatzidis. Nanostructured thermoelectrics: The new paradigm? *Chemistry of Materials*, 22(3):648–659, 2010.

[65] Daniel Champier. Thermoelectric generators: A review of applications. *Energy Conversion and Management*, 140:167–181, 2017.

[66] Zhifeng Ren, Yunsheng Lan, and Qinyong Zhang. Advances in thermoelectric materials research: Looking back and moving forward. *Science*, 338(6113):371–379, 2017.

[67] Suhani Baru and Sonal Bhatia. A review on thermoelectric cooling technology and its applications. *IOP Conference Series: Materials Science and Engineering*, 912:042004, 2020.

[68] Lon E. Bell. Cooling, heating, generating power, and recovering waste heat with thermoelectric systems. 321, 2008.

[69] T. Graf, C. Felser, and S.S.P. Parkin. Simple rules for the understanding of heusler compounds. *Progress in Solid State Chemistry*, 39(1):1–50, 2020.

[70] J. Poon and T. Tritt. Thermoelectric performance of n-type half-heusler alloys. *MRS Bulletin*, 31:216–221, 2011.

[71] C. et al. Fu. Improved thermoelectric performance in tinisn-based materials by carbon addition. *Energy Environmental Science*, 8:216–222, 2015.

[72] H. et al. Xie. Cu-doped tinisn half-heusler thermoelectric materials with enhanced zt. *Applied Physics Letters*, 100:252101, 2012.

[73] C. et al. Fu. High band degeneracy contributes to high thermoelectric performance in p-type half-heusler compounds. *Advanced Energy Materials*, 4:1400600, 2014.

[74] W. et al. Liu. Thermoelectric property studies on fenbsb-based half-heusler compounds. *Energy Environmental Science*, 9:3612–3622, 2016.

[75] G. et al. Joshi. (ti,zr,hf)nisn-based half-heuslers for waste heat recovery: high figure of merit and mechanical robustness. *Acta Materialia*, 57:3721–3732, 2011.

[76] K. et al. Yabuuchi. Thermoelectric properties of inverse heusler compound fe2coga. *Journal of Applied Physics*, 115:083706, 2014.

[77] E. et al. Rausch. Spin-dependent thermoelectric transport in hf2vz (z = ga, in, tl). *Physical Review B*, 101:035203, 2020.

[78] T. Tritt. Thermal conductivity challenges in thermoelectrics. *MRS Bulletin*, 33:366–368, 2008.

[79] S. et al. Chen. Synthesis and characterization of double half-heusler compounds for thermoelectrics. *Journal of Materials Chemistry A*, 9:10210–10220, 2021.

[80] Shashwat Anand, Max Wood, Yi Xia, Chris Wolverton, and G. Jeffrey Snyder. Double half-heuslers. *Joule*, 3(5):1226–1238, 2019.

[81] Tanja Graf, Claudia Felser, and Stuart SP Parkin. Simple rules for the understanding of heusler compounds. *Progress in solid state chemistry*, 39(1):1–50, 2011.

[82] James E Saal, Scott Kirklin, Muratahan Aykol, Bryce Meredig, and Christopher Wolverton. Materials design and discovery with high-throughput density functional theory: the open quantum materials database (oqmd). *Jom*, 65:1501–1509, 2013.

[83] Scott Kirklin, James E Saal, Bryce Meredig, Alex Thompson, Jeff W Doak, Muratahan Aykol, Stephan Rühl, and Chris Wolverton. The open quantum materials database (oqmd): assessing the accuracy of dft formation energies. *npj Computational Materials*, 1(1):1–15, 2015.

[84] Shiyang He, Amin Bahrami, Pingjun Ying, Lars Giebeler, Xiang Zhang, Kornelius Nielsch, and Ran He. Improving the thermoelectric performance of zrni (in, sb)-based double half-heusler compounds. *Journal of Materials Chemistry A*, 10(25):13476–13483, 2022.

[85] Z Charifi, H Baaziz, ŞULE Uğur, and GÖKAY Uğur. Prediction of the electronic structure, optical and vibrational properties of scxco2sb2 (x= v, nb and ta) double half-heusler alloys: a theoretical study. *Indian Journal of Physics*, 97(2):413–428, 2023.

[86] Amel Slamani, Friha Khelfaoui, Oufaa Sadouki, Abdelkader Bentayeb, Keltouma Boudia, and Fadila Belkharroubi. Structural, mechanical, electronic, and thermoelectric properties of tizrco2bi2, tihfco2bi2, and zrhfco2bi2 double half heusler semiconductors. *Emergent Materials*, 6(2):681–690, 2023.

[87] Saber Saad Essaoud, Abdelmadjid Bouhemadou, Missoum Radjai, Mohammed Elamin Ketfi, Djamel Allali, Saad Bin-Omran, and S Maabed. First-principles analysis of the structural, thermodynamic, elastic and thermoelectric properties of luxco2sb2 (x= v, nb and ta) double half heusler alloys. *Inorganic Chemistry Communications*, 159:111733, 2024.

[88] Saber Saad Essaoud, Abdelmadjid Bouhemadou, Djamel Allali, Mohammed Elamin Ketfi, Missoum Radjai, and Saad Bin-Omran. An ab initio investigation of the structural stability, thermodynamic, optoelectronic, and thermoelectric properties of luxni2sn2 (x= v, nb, ta) double half heusler materials. *Journal of Inorganic and Organometallic Polymers and Materials*, 34(2):885–902, 2024.

[89] A.N. Filanovich, A.V. Lukoyanov, and A.A. Povzner. Electronic structure and elastic properties of double half-heusler thermoelectric materials mgxy2z2 (x=zr/hf, y=pd/pt, z=bi/sb). *Physica B: Condensed Matter*, 669:415280, 2023.

[90] K. Bouhadjer, M. Boudjelal, M. Matougui, S. Bentata, T. Lantri, M. Batouche, T. Seddik, R. Khenata, B. Bouadjemi, S. Bin Omran, Muhammad Waqas Iqbal, and Mumtaz Manzoor. Structural, optoelectronic, thermodynamic and thermoelectric properties of double half heusler (dhh) ti2fenisb2 and ti2ni2insb compounds: A tb-mbj study. *Chinese Journal of Physics*, 85:508–523, 2023.

[91] Khadidja Berarma, Saber Sâad Essaoud, Ahmad A Mousa, Said M Azar, and Anas Y Al-Reyahi. Opto-electronic, thermodynamic and charge carriers transport properties of ta2fenisn2 and nb2fenisn2 double half-heusler alloys. *Semiconductor Science and Technology*, 37(5):055013, apr 2022.

[92] Khadidja Berarma, Saber Sâad Essaoud, Said Al Azar, Anas Y Al-Reyahi, Ahmad A Mousa, and Ahmad Mufleh. Computational characterization of structural, optoelectronic and thermoelectric properties of some double half-heusler alloys x2fey sb2 (x: Hf, zr; y: Ni, pd). *Phase Transitions*, 96(11-12):806–821, 2023.

[93] EM Elsehly, Eman N Almutib, et al. Transport and thermoelectric properties of m2fenisb2 (m= ti, hf) heusler alloys.

[94] Haonan Ding, Xiaohua Li, Yu Feng, and Bo Wu. Electronic structure, magnetism and disorder effect in double half-heusler alloy mn2fecosi2. *Journal of Magnetism and Magnetic Materials*, 555:169367, 2022.

[95] Zhou Cui, Haonan Ding, and Yu Feng. Investigation of the half-metallicity, magnetism and spin transport properties of double half-heusler alloys mn 2 cocrz 2 (z= p, as). *Physical Chemistry Chemical Physics*, 23(33):17984–17991, 2021.

[96] Oukacha Douinat, Ahmed Boucherdoud, Abdelkarim Seghier, Mohammed Houari, Smain Mesbah, Tayeb Lantri, and Benaouda Bestani. Theoretical investigation of the physical, mechanical, and thermal properties of zr2xbini2 (x: Al, ga) double half-heusler alloys. *Journal of Materials Research*, 38(20):4509–4521, 2023.

[97] Bhawna Sahni and Aftab Alam. Double half-heusler alloys x 2 ni 2 insb (x= zr, hf) with promising thermoelectric performance: The role of varying structural phases. *Physical Review Applied*, 22(3):034034, 2024.

[98] S Krishnaveni and M Sundareswari. Band gap engineering in ruthenium-based heusler alloys for thermoelectric applications. *International Journal of Energy Research*, 42(2):764–775, 2018.

[99] A. Bahrami, R. He, et al. Improving the thermoelectric performance of zrni(in,sb)-based double half-heusler compounds. *Journal of Materials Chemistry A*, 10:13476–13483, 2022.

[100] Kun Hu, Ruiwen Xie, Chen Shen, Hailong Peng, Huashan Liu, and Hongbin Zhang. High-throughput design of co-based magnetic heusler compounds. *Acta Materialia*, 259:119255, 2023.

[101] L. Bainsla and K.G. Suresh. Chapter 1 - physics and magnetism of quaternary heusler alloys. volume 25 of *Handbook of Magnetic Materials*, pages 1–66. Elsevier, 2016.

[102] M Benkabou, H Rached, A Abdellaoui, D Rached, Rabah Khenata, M Hichem Elahmar, B Abidri, N Benkhettou, and S Bin-Omran. Electronic structure and magnetic properties of quaternary heusler alloys corhmnz (z= al, ga, ge and si) via first-principle calculations. *Journal of Alloys and Compounds*, 647:276–286, 2015.

[103] Ken Kurosaki, Takuji Maekawa, Hiroaki Muta, and Shinsuke Yamanaka. Effect of spark plasma sintering temperature on thermoelectric properties of (ti,zr,hf)nisn half-heusler compounds. *Journal of Alloys and Compounds*, 397(1):296–299, 2005.

[104] Xin Liu, Shaoqin Wang, Zirui Dong, Yi Chang, Jiye Zhang, Xinyue Zhang, and Jun Luo. Discovery of (sc, v) cosb double half-heusler alloys with low lattice thermal conductivity. *Journal of Alloys and Compounds*, 1010:178078, 2025.

[105] Yilin Han, Yang Wu, Tingzhou Li, R Khenata, Tie Yang, and Xiaotian Wang. Electronic, magnetic, half-metallic, and mechanical properties of a new equiatomic quaternary heusler compound yrhtige: A first-principles study. *Materials*, 11(5):797, 2018.

[106] Jiaying Ji, Qijia Gu, Rabah Khenata, Fayang Guo, Yanfeng Wang, Tie Yang, and Xingwen Tan. Structural configuration and tetragonal phase stability in the equiatomic quaternary heusler compound tiznmnsi. *RSC advances*, 10(65):39731–39738, 2020.

[107] Muhammad Mushtaq, Muhammad Atiff Sattar, and Sajad Ahmad Dar. Phonon phase stability, structural, mechanical, electronic, and thermoelectric properties of two new semiconducting quaternary heusler alloys cocuzrz (z= ge and sn). *International Journal of Energy Research*, 44(7):5936–5946, 2020.

[108] Ying Chen, Shaobo Chen, Bin Wang, Bo Wu, Haishen Huang, Xinmao Qin, Dongxiang Li, and Wanjun Yan. Half-metallicity and magnetism of the quaternary heusler compound tizrcoin1-xgex from the first-principles calculations. *Applied Sciences*, 9(4):620, 2019.

[109] Pascal Neibecker, Markus E Gruner, Xiao Xu, Ryosuke Kainuma, Winfried Petry, Rossitza Pentcheva, and Michael Leitner. Ordering tendencies and electronic properties in quaternary heusler derivatives. *Physical Review B*, 96(16):165131, 2017.

[110] VN Uvarov, YV Kudryavtsev, EM Rudenko, NV Uvarov, AE Perekos, MP Melnik, and VY Tarenkov. Lattice site occupation effect on the electronic structure and physical properties of quaternary comncral heusler alloy. *Journal of Applied Physics*, 134(11), 2023.

[111] Enamullah, DD Johnson, KG Suresh, and Aftab Alam. Half-metallic co-based quaternary heusler alloys for spintronics: Defect-and pressure-induced transitions and properties. *Physical Review B*, 94(18):184102, 2016.

[112] Xiaotian Wang, Houari Khachai, Rabah Khenata, Hongkuan Yuan, Liying Wang, Wenhong Wang, Abdelmadjid Bouhemadou, Liyu Hao, Xuefang Dai, Ruikang Guo, et al. Structural, electronic, magnetic, half-metallic, mechanical, and thermodynamic properties of the quaternary heusler compound fecrrusi: a first-principles study. *Scientific reports*, 7(1):16183, 2017.

[113] John C Slater. Atomic radii in crystals. *The Journal of Chemical Physics*, 41(10):3199–3204, 1964.

[114] Laura Bégon-Lours, Martijn Mulder, Pavan Nukala, Sytze De Graaf, Yorick A Birkhölzer, Bart Kooi, Beatriz Noheda, Gertjan Koster, and Guus Rijnders. Stabilization of phase-pure rhombohedral hfzr o 4 in pulsed laser deposited thin films. *Physical Review Materials*, 4(4):043401, 2020.

[115] Dongwon Shin and Zi-Kui Liu. Phase stability of hafnium oxide and zirconium oxide on silicon substrate. *Scripta materialia*, 57(3):201–204, 2007.

[116] Xiaoqing Li. *Mechanical Properties of Transition Metal Alloys from First-Principles Theory*. PhD thesis, KTH Royal Institute of Technology, 2014.

[117] Paul Larson, SD Mahanti, and MG Kanatzidis. Structural stability of ni-containing half-heusler compounds. *Physical Review B*, 62(19):12754, 2000.

[118] Lakhan Bainsla and KG Suresh. Equiatomic quaternary heusler alloys: A material perspective for spintronic applications. *Applied Physics Reviews*, 3(3), 2016.

[119] Ming Yin and Philip Nash. The effect of a fourth element (co, cu, fe, pd) on the standard enthalpy of formation of the heusler compound ni2mnsn. *Journal of Alloys and Compounds*, 667:184–190, 2016.

[120] Liefeng Feng, Jiannan Ma, Yue Yang, Tingting Lin, and Liying Wang. The electronic, magnetic, half-metallic and mechanical properties of the equiatomic quaternary heusler compounds ferhcrsi and fepdcrsi: A first-principles study. *Applied Sciences*, 8(12):2370, 2018.

[121] Himanshu Joshi, DP Rai, Lalhriatpuia Hnamte, Amel Laref, and RK Thapa. A theoretical analysis of elastic and optical properties of half heusler mcosb (m= ti, zr and hf). *Heliyon*, 5(3), 2019.

[122] Anubhav Jain, Shyue Ping Ong, Geoffroy Hautier, et al. The materials project: A materials genome approach to accelerating materials innovation. *APL Materials*, 1(1):011002, 2013.

[123] Xiaotian Wang, Houari Khachai, Rabah Khenata, Hongkuan Yuan, Liying Wang, Wenhong Wang, Abdelmadjid Bouhemadou, Liyu Hao, Xuefang Dai, Ruikang Guo, et al. Structural, electronic, magnetic, half-metallic, mechanical, and thermodynamic properties of the quaternary heusler compound fecrrusi: a first-principles study. *Scientific reports*, 7(1):16183, 2017.

[124] Joseph Ngugi Kahiu, Samuel Kimani Kihoi, Hyunji Kim, U Sandhya Shenoy, D Krishna Bhat, and Ho Seong Lee. Asymmetric thermoelectric performance tuning in low-cost zrfe x ni1–x sb double half-heusler materials. *ACS Applied Energy Materials*, 6(8):4305–4316, 2023.

[125] Xiaoxiang Shi, Weishu Liu, and Lidong Chen. Recent advances in half-heusler thermoelectric materials. *NPG Asia Materials*, 11(1):24, 2019.

[126] Krzysztof Gofryk, Edgar Bauer, Olga N. Taran, Jakub Rybak, and Andrei V. Sologub. Thermoelectric properties and atomic disorder in tifenisb double half-heusler compound. *Journal of Alloys and Compounds*, 832:154910, 2020.

[127] Jin Zhang, Chao Fu, Zhiyong Wang, Bingyun Liu, and Xinfeng Tang. Enhanced thermoelectric performance in double half-heusler compounds tinicosb via carrier engineering. *Acta Materialia*, 224:117473, 2022.

[128] Haitao Gou, Guangzhao Qin, Song Wang, Yue Chen, and Qingjie Zhang. High thermoelectric performance predicted in os-containing double half-heusler compounds. *Journal of Materials Chemistry A*, 9(31):17134–17143, 2021.

[129] Shiyang He, Amin Bahrami, Pingjun Ying, Lars Giebeler, Xiang Zhang, Kornelius Nielsch, and Ran He. Improving the thermoelectric performance of zrni (in, sb)-based double half-heusler compounds. *Journal of Materials Chemistry A*, 10(25):13476–13483, 2022.

[130] Bhawna Sahni and Aftab Alam. Double half-heusler alloys x 2 ni 2 insb (x= zr, hf) with promising thermoelectric performance: The role of varying structural phases. *Physical Review Applied*, 22(3):034034, 2024.

[131] Jian He and Terry M. Tritt. Advances in thermoelectric materials research: Looking back and moving forward. *Science*, 357(6358):eaak9997, 2017.

[132] Anubhav Jain, Shyue Ping Ong, Geoffroy Hautier, Wei Chen, William Davidson Richards, Stephen Dacek, Shreyas Cholia, Dan Gunter, David Skinner, Gerbrand Ceder, and Kristin A. Persson. Commentary: The materials project: A materials genome approach to accelerating materials innovation. *APL Materials*, 1(1):011002, 07 2013.

[133] Prashun Gorai, Vladan Stevanović, and Eric S Toberer. Computationally guided discovery of thermoelectric materials. *Nature Reviews Materials*, 2(9):1–16, 2017.

[134] Guangzhao Qin, An Huang, Yinqiao Liu, Huimin Wang, Zhenzhen Qin, Xue Jiang, Jijun Zhao, Jianjun Hu, and Ming Hu. High-throughput computational evaluation of lattice thermal conductivity using an optimized slack model. *Mater. Adv.*, 3:6826–6830, 2022.

[135] Alex Zunger. Inverse design in search of materials with target functionalities. *Nature Reviews Chemistry*, 2(4):0121, 2018.

[136] Alexander Page, P.F.P. Poudeu, and Ctirad Uher. A first-principles approach to half-heusler thermoelectrics: Accelerated prediction and understanding of material properties. *Journal of Materiomics*, 2(2):104–113, 2016. Special Issue on Advances in Thermoelectric Research.

[137] Souraya Goumri-Said, Sikander Azam, Bakhtiar Ul Haq, and Mohammed Benali Kanoun. Zintl germanides for thermoelectric applications: Insights from dft and boltzmann transport theory. *Results in Physics*, 69:108119, 2025.

[138] Seungbin Han, Dongkyu Lee, Sungwoo Lee, Gun-Do Lee, Sangyeop Lee, and Hyejin Jang. Lattice thermal conductivity and phonon transport properties of monolayer fluorographene. *Journal of Applied Physics*, 136(13), 2024.